Autophagosomes contribute to intracellular lipid distribution in enterocytes

Salem Ait Khaldoun[a], Marc-Alexandre Emond-Boisjoly[a], Danielle Chateau[a], Véronique Carrière[a], Michel Lacasa[a], Monique Rousset[a], Sylvie Demignot[a,b], and Etienne Morel[a]

[a]Centre de Recherche des Cordeliers, UMR S 872, Université Pierre et Marie Curie-Paris 6, Institut National de la Santé et de la Recherche Médicale, U 872 and UMR S 872, Université Paris Descartes-Paris 5, F-75006 Paris, France;
[b]Laboratoire de Pharmacologie Cellulaire et Moléculaire, Ecole Pratique des Hautes Etudes, F-75006 Paris, France

ABSTRACT **Enterocytes, the intestinal absorptive cells, have to deal with massive alimentary lipids upon food consumption. They orchestrate complex lipid-trafficking events that lead to the secretion of triglyceride-rich lipoproteins and/or the intracellular transient storage of lipids as lipid droplets (LDs). LDs originate from the endoplasmic reticulum (ER) membrane and are mainly composed of a triglyceride (TG) and cholesterol-ester core surrounded by a phospholipid and cholesterol monolayer and specific coat proteins. The pivotal role of LDs in cellular lipid homeostasis is clearly established, but processes regulating LD dynamics in enterocytes are poorly understood. Here we show that delivery of alimentary lipid micelles to polarized human enterocytes induces an immediate autophagic response, accompanied by phosphatidylinositol-3-phosphate appearance at the ER membrane. We observe a specific and rapid capture of newly synthesized LD at the ER membrane by nascent autophagosomal structures. By combining pharmacological and genetic approaches, we demonstrate that autophagy is a key player in TG targeting to lysosomes. Our results highlight the yet-unraveled role of autophagy in the regulation of TG distribution, trafficking, and turnover in human enterocytes.**

Monitoring Editor
Robert G. Parton
University of Queensland

Received: Jun 18, 2013
Revised: Oct 24, 2013
Accepted: Oct 25, 2013

INTRODUCTION

In mammals, alimentary lipids are absorbed by enterocytes, which are the major cell population of the intestinal epithelium. A complex and specialized process requiring polarized trafficking, signaling, and membrane-remodeling events leads to intestinal secretion of lipoproteins at the basal pole of enterocytes in lymph and then in the bloodstream (Mansbach and Siddiqi, 2010). Triglycerides (TGs), the main constituents of dietary lipids, are hydrolyzed in the intestinal lumen into fatty acid and 2-mono-acyl-glycerol, which are associated with biliary products into lipid micelles and then taken up in enterocytes by passive diffusion and/or transporters (Pan and Hussain, 2012). TGs and phospholipids are synthesized from internalized lipids and accumulate in the endoplasmic reticulum (ER) membrane bilayer. In enterocytes, the bulk of TGs can be handled by specialized ER membrane machineries in two major pathways, which, from a topological point of view, are opposed but connected (Sturley and Hussain, 2012): 1) as in most mammalian cells, the ER can produce cytosolic lipid droplets (LDs) to pack up TGs in a neutral lipid core surrounded by a monolayer of phospholipids and specific coat proteins (Martin and Parton, 2006; Fujimoto *et al.*, 2008; Thiele and Spandl, 2008); 2) as in hepatocytes, the ER of enterocytes has the ability to produce intraluminal TG-containing structures, which fuse with a single molecule of apolipoprotein B stabilized by lipidation (ApoB48 in enterocytes, ApoB100 in hepatocytes in humans), leading to the biogenesis of pre-lipoproteins in the ER lumen. Further addition of TGs, adjunction of surface apolipoproteins (ApoA4, ApoCIII, ApoA1), and subsequent trafficking through the Golgi apparatus participate in the maturation of triglyceride-rich lipoprotein (called chylomicron in enterocytes) and its secretion (Hussain *et al.*, 2005).

In mouse enterocytes and human polarized Caco-2/TC7 enterocytes cultured on microporous filters, dietary lipids supplied as complex lipid micelles rapidly induce many events related to the bidirectional segregation of TGs: TG appearance in the ER, ApoB vesicular

This article was published online ahead of print in MBoC in Press (http://www.molbiolcell.org/cgi/doi/10.1091/mbc.E13-06-0324) on October 30, 2013.

Address correspondence to: Etienne Morel (etienne.morel@inserm.fr).

Abbreviations used: ER, endoplasmic reticulum; LD, lipid droplet; PI3P, phosphoinositol-3-phosphate; PL, phospholipid; TG, triglyceride.

trafficking, and chylomicron secretion (Morel *et al.*, 2004; Chateau *et al.*, 2005; Pauquai *et al.*, 2006), as well as TGs packed in cytosolic LDs, which can contribute later to lipoprotein secretion (Robertson *et al.*, 2003; Chateau *et al.*, 2005). The study of enterocyte LDs is therefore of primary importance in understanding the regulation of polarized alimentary lipid transfer by enterocytes (Demignot *et al.*, 2013). We previously showed that the enterocyte LD equipment was cell specific and adapted to lipid metabolism in enterocytes and may in consequence participate actively in TG partitioning upon delivery of lipid micelles (Bouchoux *et al.*, 2011). However, how enterocyte LD dynamics contributes precisely to the control of intestinal lipid absorption is poorly understood, despite its implication in the overall lipid metabolism and thus in the occurrence of cardiovascular diseases (Miller *et al.*, 2011; Demignot *et al.*, 2013).

In hepatocytes, LDs can be targeted to the autophagy pathway (Singh *et al.*, 2009), raising the notion of lipophagy, by which cytosolic neutral lipids are addressed to the lysosome by the autophagy pathway (Singh and Cuervo, 2012). Moreover, inhibition of autophagy in hepatocytes leads to massive intracellular TG increase (Singh *et al.*, 2009). Acting beside endosomal transport, macroautophagy (hereafter simply referred to as autophagy) is a stress-inducible intracellular degradative pathway (Klionsky, 2007; Xie and Klionsky, 2007; Mizushima *et al.*, 2008) that selectively eliminates defective organelles, microbes, and protein aggregates by engulfing large portions of cytoplasm into a double-membrane organelle called the autophagosome. Defaults in autophagy can hence contribute to a broad spectrum of human diseases, from cancer to metabolic disorders (Mizushima *et al.*, 2008). Autophagy induction and completion are triggered by a series of complex membrane-trafficking and remodeling events: briefly, a portion of membrane coming from the ER will form an initial and specialized structure referred to as a phagophore (or isolation membrane), which will require a wide range of autophagy-related actors—including most of the ATG protein family members, local phosphatidylinositol-3-phosphate (PI3P; synthesized by Vps34/PI3KCIII at the ER membrane), beclin1, and LC3 (the mammalian homologue of yeast ATG8)—to mature as an autophagosome (Klionsky, 2007). The autophagosome will then fuse eventually with lysosomes so that its content is degraded (Nakatogawa *et al.*, 2009; Codogno *et al.*, 2011). Although lipophagy and the interconnection of the autophagy machinery and LDs were recently documented in hepatocytes (Ding *et al.*, 2010; Heaton and Randall, 2010; Vescovo *et al.*, 2012), macrophages (Ouimet *et al.*, 2011), and fibroblasts (Velikkakath *et al.*, 2012), this had not yet been investigated in enterocytes, despite the essential function of these specialized cells in the regulation of alimentary lipid flux via their ability to store massive amounts of lipids as LDs and/or secrete them as lipoproteins (Demignot *et al.*, 2013). One major difference between lipid metabolism regulation in hepatocytes and enterocytes resides in the extracellular lipid uptake modus operandi: whereas hepatocytes handle lipids from the bloodstream by regulated receptor-mediated endocytosis, enterocytes have to face immediate and massive lipid volumes coming from the intestinal lumen. Once lipids have entered the enterocytes, they instantly mobilize biosynthetic membranes, notably the ER membrane, which start partitioning newly synthesized lipids between the ER lumen (for lipoprotein biogenesis and secretion) and cytosolic LDs. Given that the ER is a central organelle for numerous cellular functions, including membrane dynamics and trafficking, lipid synthesis, ER-stress–mediated signaling, LD biogenesis (as well as of lipoproteins in specialized cells), and autophagosome formation, it is tempting to hypothesize that, in the enterocyte context just described, these essential cellular pathways can be interconnected. They may thus contribute in concert to the proper repartition of neutral lipids and their stock regulation after acute alimentary lipid delivery.

The aim of this study is to characterize LD behavior and trafficking upon delivery of alimentary lipids as complex lipid micelles and investigate the putative role of autophagy in LD fate in enterocytes. Using cell imaging techniques and biochemistry, we describe the heterogeneity of LD populations in enterocytes in terms of size and subcellular localizations. We demonstrate that nascent LDs remain associated with ER membrane within the first hour after lipid delivery and that a stock of LDs is formed later, at the basal pole of cells. Lipid micelles induce in parallel a very rapid autophagic response, accompanied by the onset of PI3P-labeled ER membranes corresponding to autophagosomal primary structures. We show that whereas starvation-induced autophagy decreases the volume and number of LDs, RNA interference (RNAi)–mediated inhibition of autophagy, as well as chemical blockade of a lysosomal acid lipase, triggers massive LD increase, demonstrating for the first time that autophagy is required for LD breakdown by lysosomes in enterocytes after lipid supply. Finally, we characterize the process of LD targeting to lysosomes, which starts upon their capture by autophagosomal structures positive for PI3P and LC3 at the ER membrane, arguing for immediate "tagging" of small and still ER-associated LDs by the autophagosomal machinery within the first minutes of lipid delivery.

RESULTS

Dynamic pools of lipid droplets in enterocytes

One of the main functions of enterocytes is the polarized transfer of alimentary lipids to the internal milieu: the formation, trafficking, and fate of LDs in enterocytes have to be considered as key events in the regulation of neutral lipid storage/secretion. Accordingly, it is of primary importance to gather "time-and-space" information on LD biogenesis and repartition within the enterocyte cytoplasm. As a first approach we characterized the spatial distribution of LDs in differentiated Caco-2/TC7 cells supplied for 24 h with lipid micelles. As illustrated by a three-dimensional (3D) view and *XZ* projection of BODIPY-labeled structures, 24 h after lipid supply the LD population is heterogeneous in size and distribution within the cell (Figure 1A, 3D view from apical side of the cells; Figure 1F, *XZ* projection). We identified three main LD populations: perinuclear LDs (Figure 1, B, C, and F), intranuclear LDs (Figure 1, D and F), and basal LDs (Figure 1, E and F). Of interest, the perinuclear pool of LDs is often associated with the ER marker calnexin (CLNX), as illustrated in Figure 1C and Supplemental Figure S1A. Both basal and perinuclear LDs were found to be positive for the LD-associated protein perilipin2 (PLIN2/ADRP; Supplemental Figure S1B). On the basis of analysis of confocal fluorescence microscopy images, we quantified the average volume (in micrometers cubed; see *Materials and Methods*) of each LD population as a function of lipid micelle delivery time. We noticed that intranuclear LD volume was not modified upon micelle delivery, whereas both perinuclear and basal LD volume evolution was highly dependent on the treatment (Figure 1G): perinuclear LDs grew very rapidly within the first 10 min of incubation with lipid micelles, and basal LDs started growing within the first hour. Moreover, the mean volume of basal LDs was much higher than the volume of perinuclear LDs after 24 h of lipid micelle treatment, and the formation of this basal stock of LDs appeared to be microtubules dependent since its formation was inhibited by nocodazole (Figure 1H).

Together these data indicate that LD populations are dynamic and heterogeneous in polarized enterocytes and LDs seem to grow from the ER/perinuclear region, fuse, traffic via microtubules, and form stocks of neutral lipids at the basal pole of the cells.

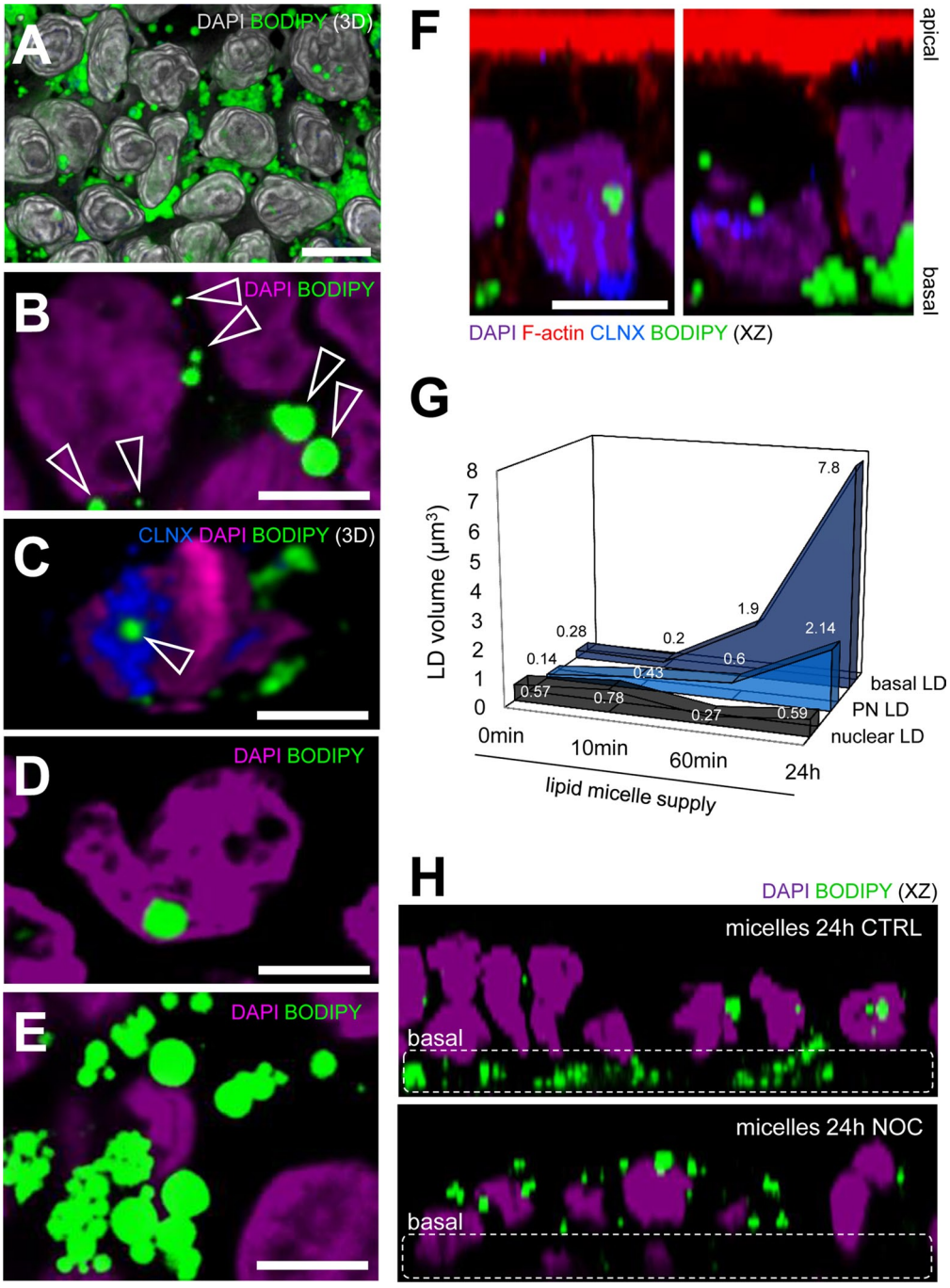

FIGURE 1: Dynamic pools of lipid droplets in polarized enterocytes after lipid micelle supply. (A–F) Polarized and differentiated Caco-2/TC7 enterocytes were cultured on microporous filters for 14 d, and lipid micelles were delivered to the apical compartment for the last 24 h before fixation. (A) A 3D view of BODIPY-labeled LD distribution in Caco-2/TC7 cells. Scale bar, 10 µm. (B) Fixed cells stained with BODIPY and DAPI and analyzed by confocal microscopy. The perinuclear zone is shown; arrowheads indicate LDs in the vicinity of the nucleus. (C) Fixed cells stained with BODIPY, DAPI, and anti-CLNX antibody and analyzed by confocal microscopy. The 3D perinuclear zone is shown. The arrowhead indicates LD associated closely with a CLNX-positive perinuclear endoplasmic reticulum structure. (D) Cells processed as in B. An intranuclear LD. (E) Fixed cells stained with BODIPY and DAPI and analyzed by confocal microscopy. The basal zone is shown. Scale bars, 4 µm (B–E). (F) Fixed cells stained with BODIPY, DAPI, anti-CLNX antibody, and fluorescent-phalloidin (F-actin). The *XZ*-projection of *XY*-stack acquisitions in two different fields, illustrating the presence of LDs at the basal pole of the cells, in the perinuclear vicinity, and inside nucleus. Scale bar, 12 µm. (G) Polarized and differentiated Caco-2/TC7 enterocytes treated with lipid micelles for the indicated times and fixed and stained with BODIPY, as in A–F. Confocal acquisitions were analyzed using the BODIPY signal. The mean volume of LD (in μm^3) was quantified in each condition for intranuclear (nuclear LD; gray), perinuclear (PN LD; light blue), and basal LDs (dark blue) and represented graphically ($n = 5$ independent experiments). (H) Polarized and differentiated Caco-2/TC7 enterocytes treated with lipid micelles for 24 h in presence (NOC) or absence (CTRL) of nocodazole, fixed, and stained with DAPI and BODIPY. The *XZ*-projection of *XY*-stack acquisitions is shown in both conditions.

Alimentary lipid supply triggers autophagic response in enterocytes in vivo and in vitro

Autophagy is involved in cytosolic LD clearance in hepatocytes, a phenomenon described as macrolipophagy (Singh *et al.*, 2009; Singh and Cuervo, 2012; Weidberg *et al.*, 2009). Hepatocytes and enterocytes share the ability to deal with large amounts of neutral lipids, and they both have triglyceride-rich lipoprotein synthesis machinery located at the ER membrane (Mansbach and Siddiqi, 2010). However, lipid delivery to each cell type is different. We thus wondered whether acute delivery of dietary lipids to enterocytes could induce an autophagic response. We first addressed this question in vivo using mice fed a standard meal or a meal supplemented with 150 µl of olive oil, which induces massive cytosolic LD appearance in mouse enterocytes (Bouchoux *et al.*, 2011). Mouse intestinal epithelium was recovered, and lipidated LC3 ($LC3_{II}$) was analyzed by SDS–PAGE/Western blot. LC3-II is the posttranslationally modified form of LC3, which is associated with autophagosome membranes and can be distinguished from its precursor, LC3-I, by SDS–PAGE because of its increased electrophoretic mobility (apparent molecular weight of 16 kDa for LC3-I vs. 14 kDa for LC3-II; Kabeya *et al.*, 2000). We found that the amount of $LC3_{II}$ was increased 60 min (unpublished data) and 180 min (Figure 2, A and B) after food intake in mice fed the oily meal as compared with mice fed standard meal, suggesting that oil delivery was sufficient to induce an autophagic response in enterocytes in vivo. For further analysis, we used the differentiated human Caco-2/TC7 enterocytes supplied or not with complex lipid micelles in the apical medium. We first observed by light microscopy that a 24-h lipid micelle treatment induced a threefold increase in the number of LC3 autophagosome-related dotted structures (Mizushima *et al.*, 2010) when compared with the control condition (Figure 2, C and D). A similar increase was observed after 60 min of micelle exposure and, to a lesser extent, at short times (2 and 10 min; Figure 2, C and D). Accordingly, biochemical analysis revealed that, as observed in mice, amount of $LC3_{II}$ increased in cells treated with micelles for 24 h compared with control cells (Figure 2, E and F, top). Moreover, other key autophagy players were affected by 24-h micelle treatment: beclin1, Vps34, and ATG5 were up-regulated, whereas control proteins, such as membrane-associated annexin A2 (anxA2) and epithelial adherens junctions–associated E-cadherin (E-cadh), were not affected (Figure 2, E and F). These data argue for a specific autophagic response to micelle supply, without any cytotoxic effect, as measured by lactate dehydrogenase (LDH) release (unpublished data) and no deleterious effect on enterocyte polarization and cell–cell junctions (unpublished data and Figure 2E, E-cadh). Of interest, we found that autophagy was induced almost instantly, as early as 2 min after micelle application (Figure 2, G and H). Wortmannin (Wort), which specifically blocks Vps34 enzymatic activity and inhibits the synthesis of PI3P (a membranous lipid transiently required for autophagosome formation at the ER; Axe *et al.*, 2008; Simonsen and Tooze, 2009; Matsunaga *et al.*, 2010; Noda *et al.*, 2010), abolished LC3 lipidation, even in the presence of lipid micelles (Figure 2, G and H, 60 min + Wort condition). The latter finding shows that the increase of $LC3_{II}$ observed in our experimental conditions is directly related to autophagy. This was confirmed by a flux experiment using bafilomycin A1 (BAF.A1; Supplemental Figure S2A), which inhibits autophagosome/lysosome fusion, thus blocking the $LC3_{II}$ signal decrease induced by lysosomal degradation. Finally, we show that the autophagic response induced by lipid micelles was accompanied by a decrease of the mammalian target of rapamycin (mTOR) targets (Mizushima *et al.*, 2010) phospho-ULK1 (Ser-757) and phospho-p70 S6kinase (Thr-389; Supplemental Figure S2B), suggesting that, as for starvation-induced autophagy (Codogno *et al.*, 2011), the mTOR pathway is implicated in lipid micelle–triggered autophagy in enterocytes.

The autophagic response induced by lipid micelles is associated with perinuclear PI3P

Given that we observed that lipid-dependent autophagy in enterocytes can be inhibited by wortmannin, we monitored PI3P in the same cellular setup. We used an indirect fluorescence-based imaging assay combining the FYVE-$FYVE^{GST}$ recombinant protein and a fluorescein isothiocyanate (FITC)–anti-glutathione *S*-transferase (GST) antibody as a dye for membranous pools of PI3P because the FYVE domain binds specifically to PI3P (Gillooly *et al.*, 2000; Stenmark *et al.*, 2002). However, PI3P is mainly associated with endosomes in mammalian cells (Gruenberg and Stenmark, 2004; Lindmo and Stenmark, 2006) primarily acts as a major regulator along the endocytic pathway, where it recruits numerous endosomal actors, ensuring proper membrane dynamic events on early and late endosomes (Di Paolo and De Camilli, 2006). We essentially observed two pools of PI3P in polarized Caco-2/TC7 enterocytes: a major pool (Supplemental Figure S3A1) localized beneath the brush border domain in the subapical compartment (known to be enriched in biosynthetic and endocytic pathways associated organelles; Hoekstra *et al.*, 2004) and a minor pool at the perinuclear level in areas positive for the ER marker CLNX (Supplemental Figure S3A2). Confocal immunofluorescence microscopy analysis revealed that the subapical pool of PI3P is strongly associated with the early endosomal marker EEA1, as expected, and slightly with the late endosomal marker LAMP1 (Supplemental Figure S3B, insets). On the contrary, the small pool of vesicular PI3P observed at the perinuclear level in the vicinity of ER was not associated with EEA1 (Supplemental Figure S3C), indicating that these PI3P-positive organelles are not endosomes. PI3P can also be detected, albeit more rarely, on autophagosomal-related structures positive for both LC3 and LAMP1 (Figure 3A), making FYVE-$FYVE^{GST}$ a useful tool to label nonendosomal PI3P as well. Given that the primary membranous structure(s) of autophagosomes originate(s) from the ER (Axe *et al.*, 2008; Walker *et al.*, 2008; Hayashi-Nishino *et al.*, 2009; Yla-Anttila *et al.*, 2009), we analyzed the colocalization of LC3 with the perinuclear pool of PI3P. Indeed, vesicular PI3P was found to colocalize with LC3 with or without the ER marker CLNX (Supplemental Figure S3, D, solid arrowheads, and E, empty arrowhead, respectively). The absence of early endosomal marker and the presence of LC3 strongly suggested that the minor pool of PI3P-associated membranes observed in the vicinity or even tightly associated with ER membrane (Figure 3B) is made up of autophagy-related organelles. We then monitored the dynamic evolution of this perinuclear pool of PI3P in a time course of lipid micelle delivery in polarized Caco-2/TC7 enterocytes. To study precisely and rigorously the autophagy-associated PI3P synthesis, we transfected cells with RNAi targeting Beclin1 or ATG14 (Zeng *et al.*, 2006; Cao and Klionsky, 2007; Simonsen and Tooze, 2009; Boya *et al.*, 2013), two essential regulators of autophagosome biogenesis, which act as partners for Vps34 kinase function on nascent autophagosomal membrane (Figure 3, C and D). Whereas in Caco-2/TC7 enterocytes treated with wortmannin the subapical PI3P pool (identified as endosomal PI3P; Supplemental Figure S3) is almost completely absent, this is not the case in cells transfected with RNAi for Beclin1 or ATG14 (Figure 3E), showing that the down-regulation of Beclin1 or ATG14 has no significant effect on endosomal PI3P synthesis. To study dynamically the enterocyte response to lipid micelles, we submitted polarized Caco-2/TC7 enterocytes to a 5-min lipid micelle pulse followed or not by

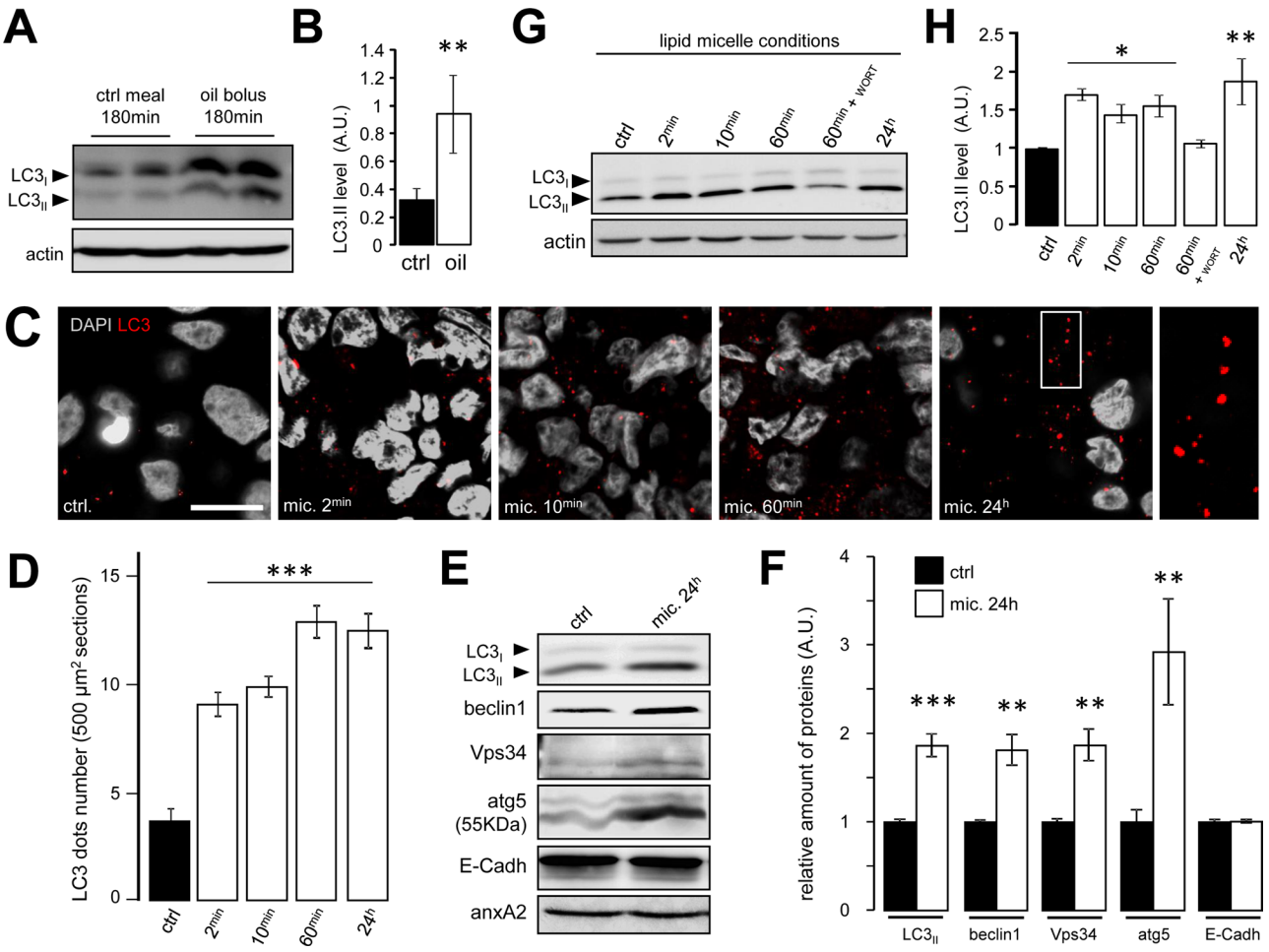

FIGURE 2: Alimentary lipid supply triggers an autophagic response in enterocytes in vivo and in vitro. (A, B) C57Bl6 mice fed a standard diet were challenged or not with an olive oil bolus (150 µl) and killed after 3 h. The isolated epithelial cells from the jejunum were analyzed by Western blotting with anti-LC3 and anti-actin as control loading marker. Signals were quantified (bar diagram, B). LC3II corresponds to the lipidated autophagosome-associated form of the LC3 protein. The bar diagram shows the quantification of the $LC3_{II}$ signal reported to actin in the indicated conditions (AU, arbitrary units). Values denote means ± SEM ($n = 3$ independent experiments; four mice for control and four mice for olive oil treatment in each experiment; $p < 0.01$). (C, D) Caco-2/TC7 enterocytes were supplied with lipid micelles for 2 min, 10 min, 60 min, 24 h or not (ctrl). Cells were fixed and stained for LC3 and DAPI and processed for confocal analysis. The inset in C shows a magnified view of the dotted signal of LC3 corresponding to autophagosomes. A quantification of the mean number of LC3 dots/500 µm² is represented in the bar diagram (D, from nuclear plan). Values denote means ± SD; $n = 40$ cells in each condition; $p < 0.001$. Scale bar, 10 µm. (E, F) Western blot analysis of autophagy-related components ($LC3_{II}$, beclin1, Vps34, and atg5) in Caco-2/TC7 enterocytes supplied with lipid micelles for 24 h (mic 24h) or not (ctrl). E-cadherin (E-cadh) was used as a marker of epithelial viability, and annexin A2 (anxA2) is used as equal loading marker, as quantified in the bar diagram (F). Values denote means ± SEM ($n = 3$ independent experiments; $^{**}p < 0.01$, $^{***}p < 0.001$). (G, H) Western blot analysis of endogenous LC3 and actin, as equal loading marker, in Caco-2/TC7 enterocytes supplied with lipid micelles for the indicated times. Wortmannin (WORT, 100 nM final) was used as Vps34/PI3KCIII pharmacological inhibitor. The bar diagram (H) shows the quantification of the $LC3_{II}$ signal reported to actin in the indicated conditions (AU, arbitrary units). Values denote means ± SEM ($n = 6$ independent experiments; $^{*}p < 0.05$, $^{**}p < 0.01$).

10-, 30-, and 60-min chase in fresh apical medium. The cells were fixed at indicated conditions, labeled with FYVE-$FYVE^{GST}$ (as shown in Figure 3B), and analyzed by confocal fluorescence microscopy for quantification of the perinuclear PI3P signal with 4′,6-diamidino-2-phenylindole (DAPI) and CLNX as nucleus and ER countermarkers, respectively. The results showed that the perinuclear pool of PI3P briefly peaks after micelle application and rapidly goes back to control values (Figure 3F, CTRL condition). Such a perinuclear PI3P peak was observed in neither cells treated with wortmannin nor in cells down-regulated for Beclin1 or ATG14 (Figure 3F). These results indicate that lipid micelles induced an immediate onset of PI3P-positive membranes emerging from the ER, which correlates with the almost immediate autophagic response characterized by LC3 lipidation in the vicinity of the ER (Figure 2G).

Newly synthesized lipid droplets are captured by autophagosomal structures at the endoplasmic reticulum membrane

Because alimentary lipid supply triggered autophagy (Figure 2), we hypothesized that autophagosomes might be directly involved in

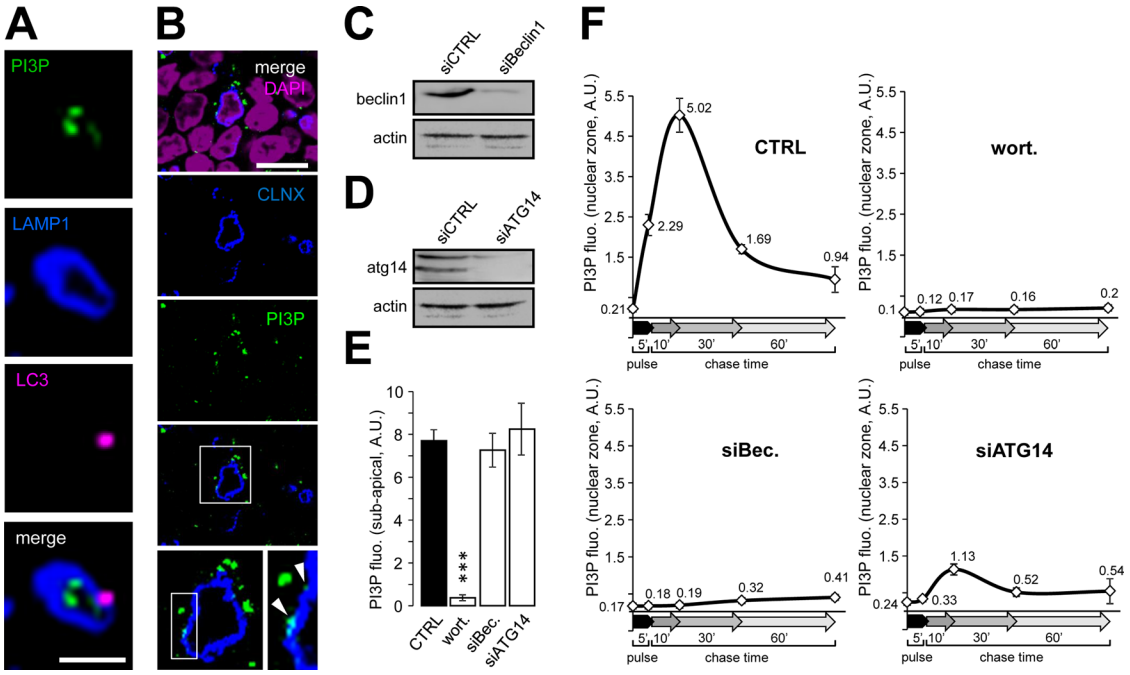

FIGURE 3: The lipid micelle–triggered autophagic response is associated with PI3P. (A) Confocal microscopy analysis of a PI3P-autophagosome related structure from a fixed Caco-2/TC7 cell. LC3 is used as a marker for autophagosome and LAMP1 for late endosome/lysosome. PI3P was stained by FYVE-FYVE^{GST} indirect fluorescence. Scale bar, 2 μm. (B) Confocal microscopy analysis of Caco-2/TC7 enterocytes treated for 1 h with lipid micelles before fixation and staining for PI3P (with FYVE-FYVE^{GST}) and CLNX as a marker for the ER. Note that PI3P domains are clearly visible at the surface of the ER (indicated by arrowheads in the inset [bottom], showing a magnified view of the ER). Scale bar, 10 μm. (C, D) Caco-2/TC7 enterocytes were transfected with mock RNAi (siCTRL), RNAi for hBeclin1 (siBeclin1, C), or RNAi for hATG14 (siATG14, D), cultured on filters, lysed, and analyzed by Western blotting with the indicated antibodies. (E) Caco-2/TC7 enterocytes cultured in the presence of wortmannin (wort, 100 nM final) or not, or transfected with RNAi for ATG14 (siATG14) or Beclin1 (siBec), were fixed and stained for PI3P with FYVE-FYVE^{GST}. The subapical PI3P-associated fluorescence intensity was quantified (in 300 × 300 pixels of subapical domain, using ImageJ software [National Institutes of Health, Bethesda, MD]) in the conditions mentioned and reported in a bar diagram. Values denote means ± SEM (n = 50 cells in each condition; $p < 0.001$). (F) Caco-2/TC7 enterocytes were submitted to a 5-min lipid micelle pulse before fixation after the indicated chase times (10, 30, and 60 min) and staining (as in B) in control conditions (CTRL) or after treatment with wortmannin (wort), siBeclin1 (siBec), or siATG14. The PI3P-ER–associated fluorescence intensity (from nuclear zone) was quantified (in 300 × 300 pixels of nuclear zone, using ImageJ) as shown (AU, arbitrary units). Values denote means ± SEM (n = 60 cells by point).

LD capture and potential trafficking to lysosomes. We thus analyzed the colocalization of LDs and autophagosomes in Caco-2/TC7 cells upon lipid micelle supply. BODIPY was used as LD marker and LC3 and LAMP1 as markers of autophagosomes and late endosomes/lysosomes, respectively. We detected colocalization between BODIPY and each of LC3 and LAMP1, as well as triple colocalization of BODIPY, LC3, and LAMP1 (Supplemental Figure S4, A and B). In most situations, LC3 and LAMP1 were detected at the periphery of the LD (Figure 4A). Moreover, electron microscopy analyses revealed that a subset of cytosolic LDs, observed after 1 h of lipid micelle supply, were included in large and double-membrane organelles, which contained cytosolic material (such as mitochondria), demonstrating that these giant organelles were autophagosomes rather than organelles from the endocytic pathway (Figure 4B). This was confirmed by immunofluorescence analysis showing absence of colocalization between EEA1- and LC3-positive LDs (which excludes early endosome–mediated transport of LDs to lysosomes), whereas LC3-positive LDs colocalized with lysobisphosphatidic acid (Matsuo *et al.*, 2004), a lipid that is only detected on late endosomes/lysosomes (unpublished data). Finally, we observed that autophagosomal membranes markers such as $LC3_{II}$ and ATG5 were associated with a purified LD fraction (as already shown for LC3; Shibata *et al.*, 2009) and enriched in such a fraction after lipid micelle delivery (Figure 4, C and D). These results show that LDs can presumably be captured by autophagosomes and subsequently fuse with late endosomes for degradation.

We further investigated the kinetics of the LD-autophagosome/autophagolysosome pathway by quantifying the organelle colocalizations upon different durations of lipid micelle treatment. We systematically quantified and classified the association of BODIPY-positive LD with either LC3 or LAMP1, both LC3 and LAMP1, or none of them from confocal microscopy fluorescence acquisitions (illustrated in Supplemental Figure S4A). Whereas <4% of the total LD population was positive for any of the two markers or both after 2 min of lipid micelle supply (with a majority of LD-LC3 colocalizations), >50% of LDs were associated with autophagosomal or autophagolysosomal markers after 60 min of incubation with lipid micelles (Figure 5A), that is, when newly synthesized LDs began to grow and emerge from the ER membrane (Figure 1). After 24 h of lipid micelle treatment, which induces a massive accumulation of LDs, a similar ratio (57%) of LDs associated with one or both markers was observed (Figure 5A). Of interest, the percentage of LD associated only with

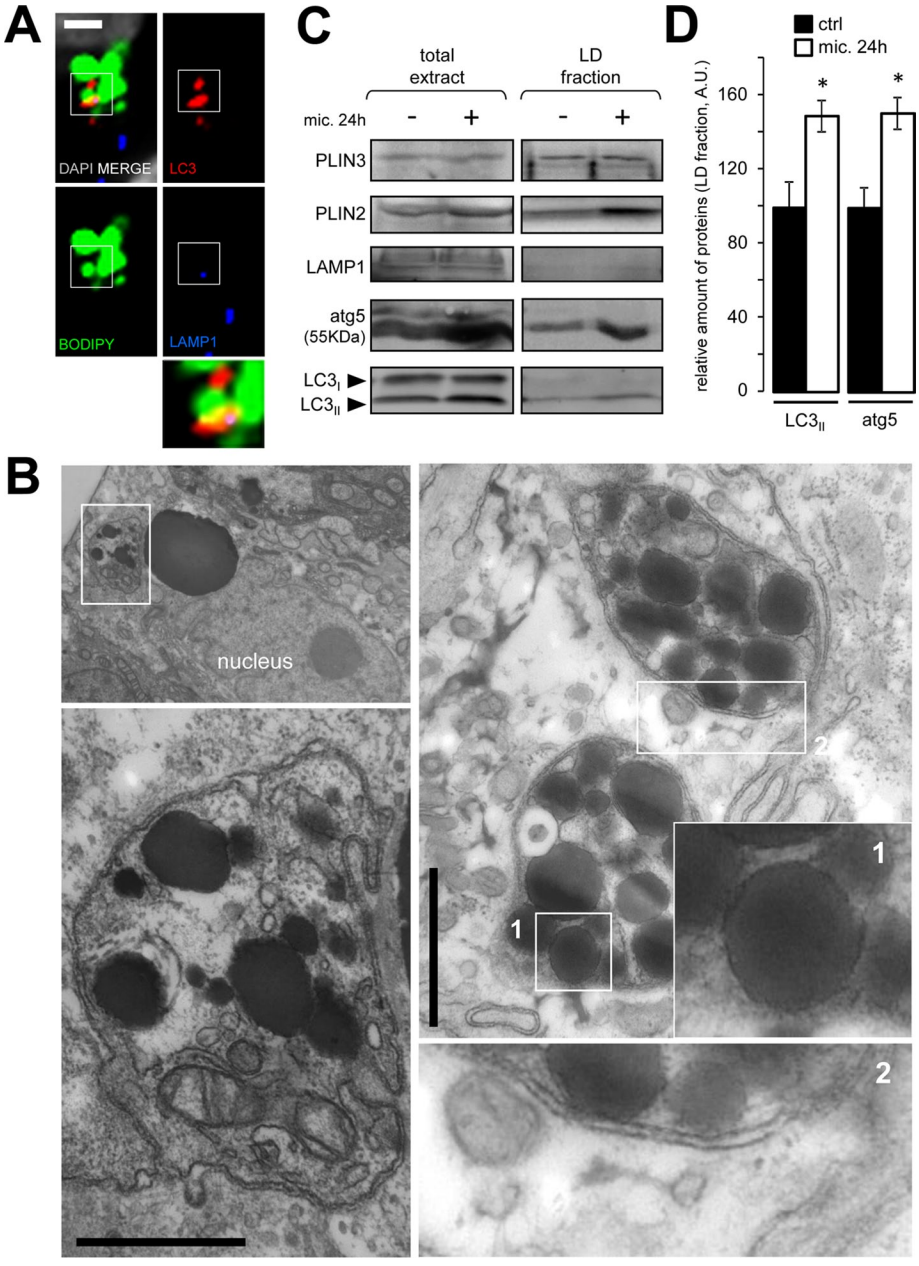

FIGURE 4: Lipid droplets and autophagosomes. (A) Confocal analysis of Caco-2/TC7 enterocytes treated with lipid micelles for 24 h before fixation and staining with the indicated antibodies and BODIPY. A larger view (inset) of the merge signal is shown in the last panel. Scale bar, 3 µm. (B) Electron microscopy analysis of Caco-2/TC7 enterocytes treated with micelles for 1 h before fixation. Inset 1, a magnified view of a LD inside the lumen of an autophagosome; inset 2, a magnified view of a double membrane reminiscent of an autophagosome. Scale bar, 2 µm. (C, D) Western blot analysis of LD fraction from Caco-2/TC7 enterocytes treated with lipid micelles for 24 h (mic. 24 h) or not. Cells were lysed (total extracts) or homogenized for flotation to collect the LD fraction. Equal volumes of fractions were analyzed with the indicated antibodies: anti-PLIN3/TIP47 and anti-PLIN2/ADRP as LD markers, ATG5 and LC3 as autophagy markers, and LAMP1 as late endosome/lysosome marker. Note the presence of ATG5 and LC3II in the LD fractions and their enrichment after 24 h of lipid micelle treatment. LC3II and ATG5 signals were quantified, and protein amounts are represented in a bar graph (D). Values denote means ± SEM ($n = 3$ independent experiments; $p < 0.05$).

LC3 dropped from 26.5 to 21%, whereas the percentage of LD associated with both LC3 and LAMP1 almost doubled, from 15.4 to 30%. These results suggest that LDs act as classic autophagosomes cargoes, with an increase of LC3/LAMP1-LD colocalization after 24 h of lipid micelle delivery, arguing for a maturation of autophagosomes (labeled with LC3) to autophagolysosomes (labeled with LAMP1, with or without LC3).

We next analyzed the site of LD capture by autophagosomes. LDs assemble and bud off the ER membrane (Robenek *et al.*, 2006; Thiele and Spandl, 2008), and we detected them often in the vicinity of rough ER membrane by electron microscopy (Supplemental Figure S6A) and light microscopy (Figure 1). Given that BODIPY did not allow us to monitor properly and dynamically LD biogenesis after a short-time delivery of lipid micelles because of the presence of preexisting LDs, we used micelles containing a fluorescent C_{12}-fatty acid (referred to as FA^{568}, for fatty acid 568 nm, associated with red fluorescence) to track the biogenesis and maturation of newly synthesized LDs within the cells after lipid micelle delivery. FA^{568} was recovered in BODIPY-positive small LDs 10 min after lipid micelle application, only in the perinuclear/CLNX-positive region of the cell (Supplemental Figure S5). Later, FA^{568}-positive LDs ("red droplets") grew and trafficked normally, as observed at 60 min and 24 h (Supplemental Figure S5), indicating that the use of FA^{568} is a powerful tool for tracking newly synthesized LD in enterocytes. We confirmed subsequently the colocalizations that we observed and quantified by using BODIPY: after 24 h of FA^{568}-micelles, FA^{568}-LDs were often associated with LC3 and/or LAMP1 (Figure 5B). By multiple and differential costaining, including the ER-PI3P (Figure 3), we analyzed whether such events also occurred after a short (2 min) or a longer (60 min) period of FA^{568}-containing lipid micelle treatment. Of interest, we found that FA^{568}-labeled LDs were associated with LC3 and PI3P and surrounded by LAMP1 after 60 min of lipid micelle treatment (Figure 5C, right), confirming the data in Figure 5A, which showed hybrid LD organelles positive for both the "early-autophagy" markers LC3 and PI3P and the "late-autophagy" marker LAMP1. The detection of PI3P on these structures strongly suggests that the dynamic pool of autophagy-related organelles observed after lipid micelle supply (Figure 3) might participate in LD capture. Indeed, we found that newly synthesized LDs that were still associated with the ER membrane (labeled with CLNX) were positive for PI3P and LC3 but negative for LAMP1 after 2 min of micelles supply (Figure 5C, left and middle). This suggests that LD-autophagy organelles form sequentially: a subset of newly formed LDs is immediately captured by PI3P and LC3-positive ER membrane domains, presumably primary autophagosomal structures, whereas LAMP1 recruitment occurs later

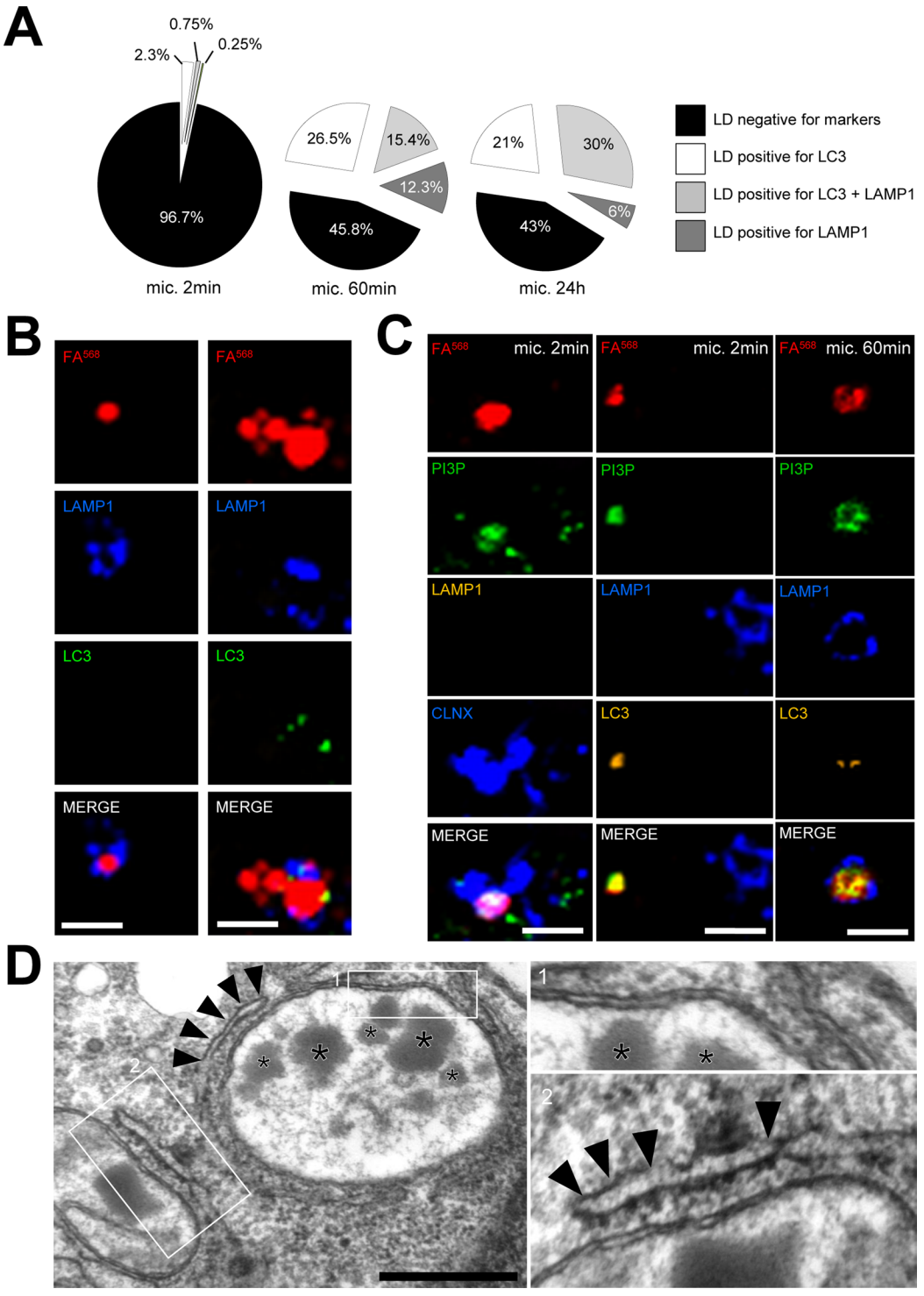

FIGURE 5: Kinetics of lipid droplet capture by autophagosome-related organelles. (A) Pie chart of confocal acquisition and quantification analysis of Caco-2/TC7 enterocytes supplied with lipid micelles for 2 min, 60 min, or 24 h before fixation and labeling with BODIPY, anti-LC3, and anti-LAMP1. The following groups of LD are expressed as percentage of total LDs for each condition: LD negative for LC3 and LAMP1, LD positive for LC3 or LAMP1, and LD positive for both LC3 and LAMP1 ($n = 6$ independent experiments). (B) Confocal analysis of Caco-2/TC7 enterocytes supplied with fluorescent fatty acid (FA^{568})–containing lipid micelles for 24 h before fixation and staining with the following antibodies or dyes: FYVE-$FYVE^{GST}$ (PI3P), anti-CLNX, anti-LC3, and anti-LAMP1. Scale bar, 4 µm. (C) Confocal analysis of Caco-2/TC7 enterocytes treated with FA^{568}-containing lipid micelles for 2 or 60 min before fixation and labeling with the indicated antibodies and dyes. Note the presence of FA^{568}-LD–positive structure associated with calnexin, PI3P, and LC3 upon 2 min of lipid micelle treatment and the quadruple colocalization of FA^{568}, PI3P, LC3, and LAMP1 at 60 but not 2 min of lipid micelle treatment. Scale bar, 3 µm. (D) Caco-2/TC7 enterocytes were supplied with lipid micelles, fixed, and processed for electron microscopy analysis (stars, LDs; arrowheads, rough ER). Note the vicinity of LD-containing autophagosomes with ER structures. Scale bar, 400 nm.

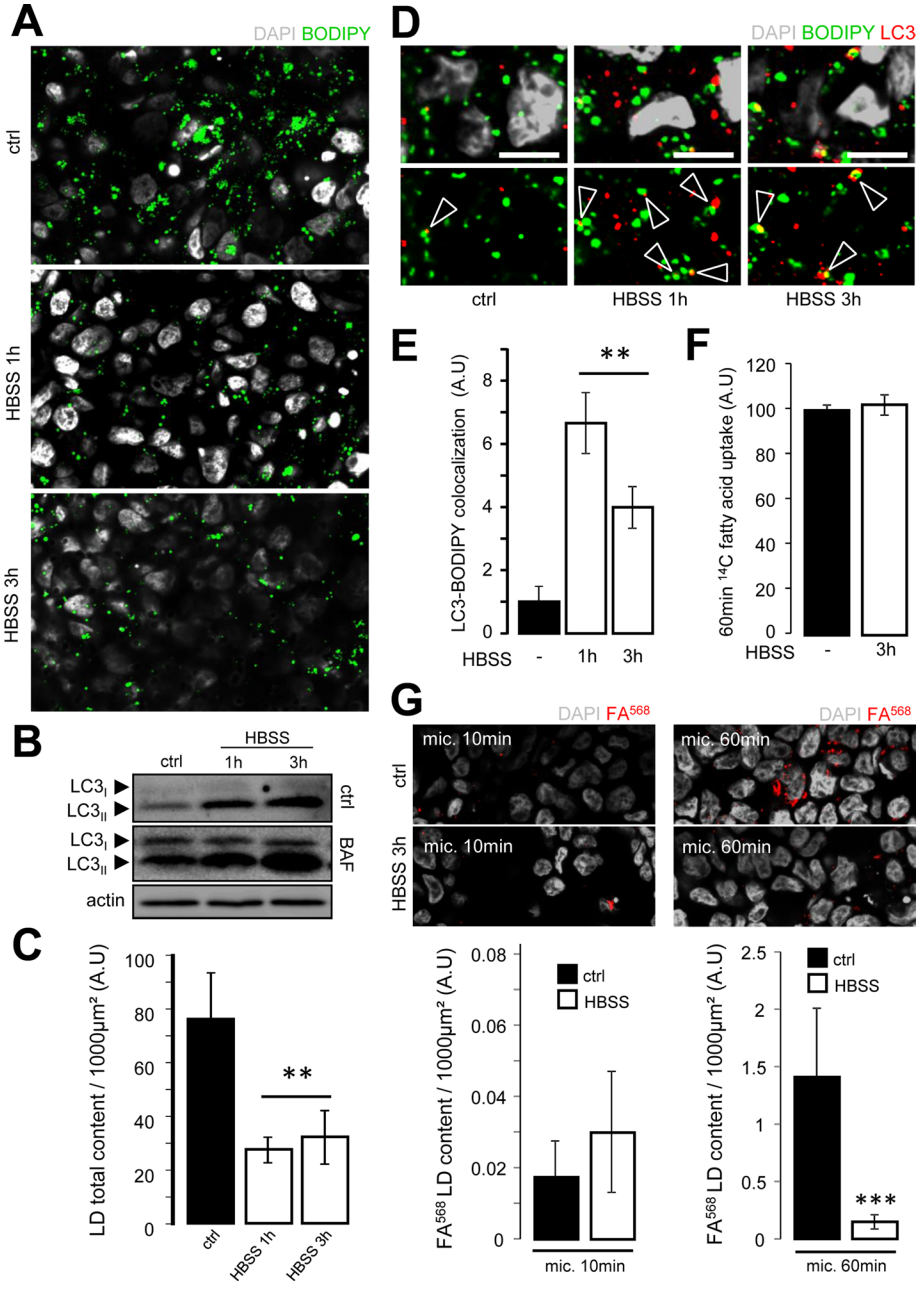

FIGURE 6: Starvation promotes a decrease in the lipid droplet total content. (A, B) Analysis of Caco-2/TC7 enterocytes starved in HBSS for the indicated times or not (ctrl), treated or not with bafilomycin (BAF, 100 nM final, for flux analysis in Western blot analysis), and stained with DAPI and BODIPY for imaging (A) or lysed and analyzed by Western blot (B) with anti-LC3 and anti-actin antibodies. (C) Bar diagram showing total lipid droplet content quantified using the BODIPY signal (i.e., *n* [number of LDs] × *v* [mean LD volume, µm^3] for a 1000-µm^2 area) in the same conditions as in A and B (AU, arbitrary units). Values denote means ± SEM ($n = 50$ cells per condition; $p < 0.01$). (D, E) Caco-2/TC7 enterocytes were treated as described in A, fixed, and stained with DAPI, BODIPY, and anti-LC3 antibody. BODIPY-LC3 colocalizations are indicated by arrowheads (D) and quantified and represented as a bar graph (E). Values denote means ± SEM ($n = 30$ cells per condition; $p < 0.01$). (F) Caco-2/TC7 enterocytes were starved for 3 h (HBSS 3 h) and supplied with [1-^{14}C]oleic acid–containing lipid micelles for 60 min in the presence of bafilomycin A1 (to block lysosomal activity, 100 nM final) to analyze the [^{14}C]fatty acid uptake by cells. Radioactivity was counted in cell lysates in the indicated conditions. Results are expressed as percentage of control condition. Values denote means ± SEM ($n = 3$ independent experiments). (G) Caco-2/TC7 cells were cultured for 6 d in serum-free medium supplemented with insulin, transferrin, and selenium. Fluorescent fatty acid (FA^{568})–containing lipid micelles were supplied for 10 or 60 min upon 3-h starvation (HBSS) or not (ctrl) before fixation. DAPI- and FA^{568}-labeled newly synthesized LD are shown. FA^{568}-labeled LD content (*nv*/1000 µm^2) was quantified as in C (see graphs; AU, arbitrary units). Values denote means ± SEM ($n = 3$ independent experiments, $p < 0.001$).

(Figure 5, A and C). Involvement of the ER membrane in this process is thus highlighted, implying complex membrane dynamics events. Electron microscopy analyses, moreover, revealed that LD-containing autophagosomes were closely associated with the ER membrane (Figure 5D and Supplemental Figure S6, B–D). Together with the confocal microscopy data showing LDs-LC3/PI3P structure association with ER membrane, these observations indicate that the PI3P-dependent autophagy machinery can be immediately recruited to ER sites where LD biogenesis takes place and captures a subset of newly synthesized LDs as soon as they bud off the ER membrane.

Starvation-induced autophagy leads to a decrease in lipid droplet content

Data presented in Figures 4 and 5 show that LDs can be captured by autophagosomes. We thus investigated whether enforced autophagy has any effect on LD fate in enterocytes. We induced autophagy in Caco-2/TC7 cells by starving them, replacing apical and basolateral media by Hank's balanced salt solution (HBSS; see *Materials and Methods*) for the indicated times (Figure 6B; see lipidation of LC3). Cells were fixed, and LDs were labeled with BODIPY (Figure 6A). Using microscopy analysis software, we quantified the mean volume (*V*, in µm^3) and the average number (*n*) of LDs in a 1000-µm^2 surface area. By multiplying $V \times n$, we obtained an immunofluorescence-based and standardized way of monitoring the LD population in a given condition that we defined as "LD total content value." We observed a twofold decrease in the LD total content of starved cells compared with control cells (Figure 6, A and C). We then analyzed by confocal microscopy the recruitment of LC3 on BODIPY structures in the conditions described in Figure 6A. Of interest, we observed that LC3-BODIPY colocalization ratio strongly increased after starvation (Figure 6, D and E). This suggests that the decrease of LD total content observed in Figure 6, A and C, is due to autophagosome mobilization, since a starvation treatment for 3 h had no effect on lipid uptake by the cells, as observed by [^{14}C]fatty acid monitoring in cells treated also with bafilomycin A1 to block lysosomal degradation (Figure 6F). These results suggest that starvation-induced autophagy decreases the existing LD population in enterocytes.

The following step was to investigate whether starvation-induced autophagy decreases newly synthesized LDs as well, that is, LDs directly formed upon lipid micelle treatment (Figure 1). To monitor specifically

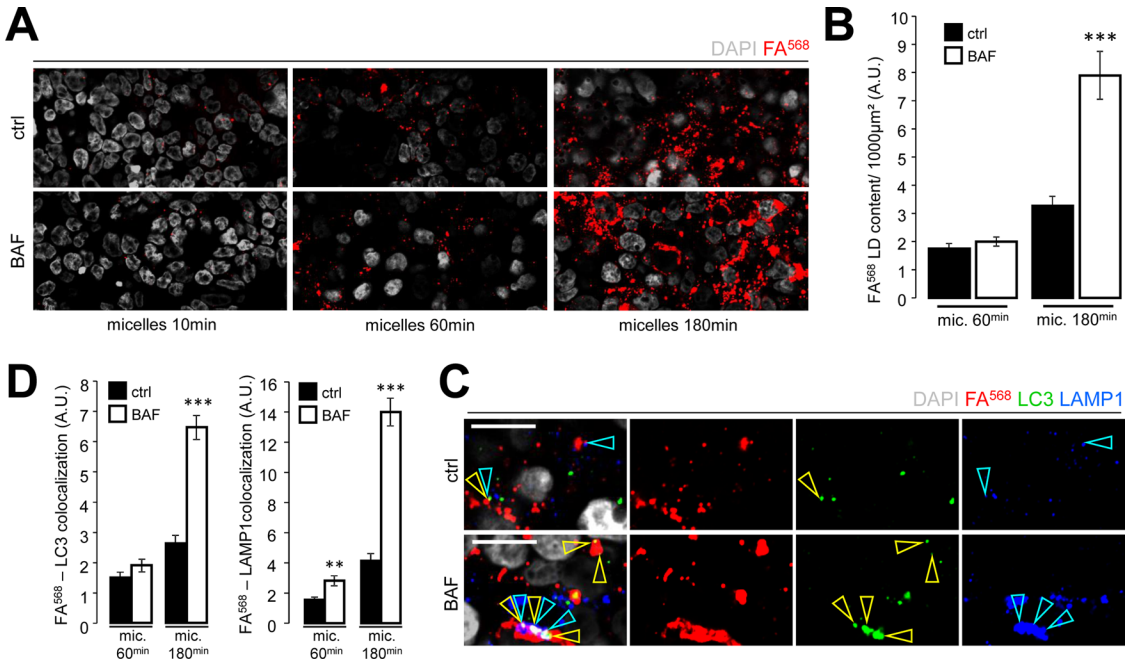

FIGURE 7: Lysosomal maturation is required for lipid droplet clearance after lipid micelle supply. (A, B) Caco-2/TC7 enterocytes were treated (BAF) or not (ctrl) for 3 h with 100 nM bafilomycin A1 to block proper autophagosome-lysosome fusion and incubated with fluorescent fatty acid (FA^{568})–containing lipid micelles for the indicated times (10, 60, or 180 min) before fixation, DAPI staining, and confocal microscopy analysis (A). FA^{568}-lipid content (*nv*/1000 µm^2) was quantified in the indicated conditions (B; AU, arbitrary units). Values denote means ± SEM ($n = 40$ cells by condition; $p < 0.001$). (C, D) Caco-2/TC7 enterocytes were treated as described in A, fixed, and stained for DAPI, LC3, and LAMP1 (scale bar, 10 µm). FA^{568} lipid droplet–LC3 and FA^{568} lipid droplet–LAMP1 colocalizations are indicated by arrowheads (yellow arrowheads for LC3, blue arrowheads for LAMP1), quantified, and represented as bar graph (D, left, for LC3; right, for LAMP1; AU, arbitrary units). Values denote means ± SEM ($n = 3$ independent experiments; $^{**}p < 0.01$, $^{***}p < 0.001$).

newly formed LDs, we used FA^{568}-micelles to study LD birth and growth after lipid micelle application (Supplemental Figure S5). To get rid of preexisting LDs, we cultured Caco-2/TC7 cells for 6 d in a serum-free medium containing insulin, transferrin, and selenium (as described in Morel *et al.*, 2004) and then exchanged the medium with HBSS for the last 3 h of culture. Cells were treated with FA^{568}-containing lipid micelles for 10 or 60 min (Figure 6G) before fixation and immunofluorescence analysis. FA^{568}-labeled LDs were then quantified from confocal acquisitions. We did not observe a significant difference in FA^{568}-LD content value after 10 min of lipid micelle application (Figure 6G, left, and graph) with or without previous starvation. However, after 60 min of FA^{568} micelle application, when newly synthesized LDs emerged from the ER membrane (Figure 1), the FA^{568}-LD content was lower in the starved condition than in the control condition (Figure 6G, right, and graph), indicating that in this condition the newly synthesized LD content was affected either by their degradation or by inhibition of their growth.

Lysosomes participate in lipid droplet regulation after lipid micelle delivery

Autophagy targets its cargoes to lysosomes for degradation/breakdown. We thus investigated the role of lysosomes in LD fate upon lipid micelle treatment of enterocytes. Caco-2/TC7 cells were treated with bafilomycin A1 (BAF) for 3 h in the presence of FA^{568}-containing lipid micelles for the indicated times (Figure 7A). BAF inhibits lysosomal acidification and fusion of autophagosomes with lysosomes, blocking the autophagic flux at the terminal step (Yamamoto *et al.*, 1998; Mizushima *et al.*, 2010). This led to accumulation of $LC3_{II}$, as seen in Supplemental Figure S2A, since autophagosomes are not degraded. FA^{568}-LD content was analyzed by fluorescence microscopy and quantified. Treatment with BAF induced a massive increase of FA^{568}-LD content value as compared with control (Figure 7, A and B) after 180 min of lipid micelle treatment but not after 60 min, suggesting that LDs require lysosome for TG degradation, starting from >60 min after the lipid micelle treatment. Moreover, we show that FA^{568}LD-LC3 and FA^{568}LD-LAMP1 colocalization ratios were strongly increased by BAF treatment (Figure 7, C and D), notably after 180 min of lipid micelle treatment.

Because the hydrolysis of TGs requires specific lipases, we focused on the lysosomal acid lipase, which hydrolyses lipids in lysosomes and requires an acid pH to be active (Ouimet *et al.*, 2011; Skop *et al.*, 2012). To investigate the effect of this lipase on LDs without affecting the lysosome itself, we used a specific pharmacological inhibitor of lysosomal acid lipase, referred to as LALi (Rosenbaum *et al.*, 2010), for lysosomal acid lipase inhibitor 2 compound 12 (see *Materials and Methods*). As with bafilomycin (Figure 7), we observed a massive increase in FA^{568}-LD content in cells treated with LALi (Supplemental Figure S7, A and B) at 180 min of lipid micelle exposure. This was specific to the lipase inhibition, since LALi had no effect on the endolysosome cargo epidermal growth factor receptor (EGFR) or late endosome/lysosome protein LAMP1 levels (Supplemental Figure S7C). Together these data show that lysosomes and the lysosomal acid lipase are involved in the degradation of a subset of newly synthesized LDs in enterocytes.

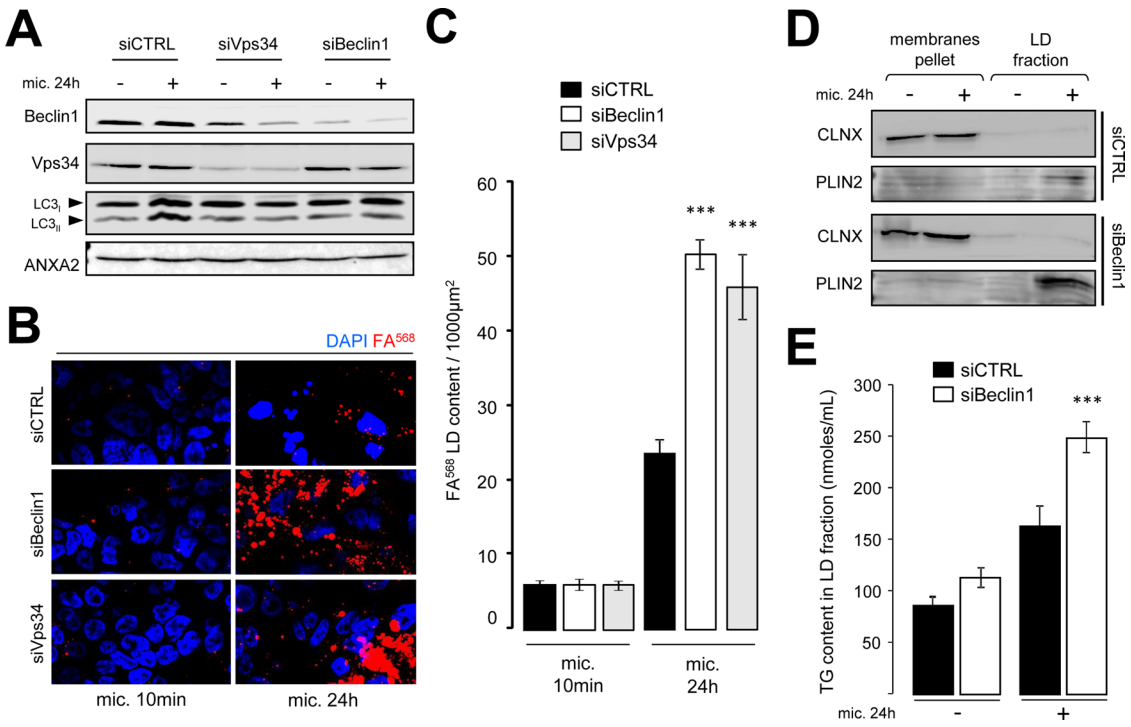

FIGURE 8: Inhibition of the primary steps of autophagy induces an increase in total lipid droplet content. (A) Caco-2/TC7 enterocytes were transfected with mock RNAi (siCTRL), RNAi for hVps34 (siVps34), or hBeclin1 (siBeclin1), plated on culture filters, and supplied with lipid micelles for 24 h (mic. 24 h) or not. Cells were lysed and analyzed by Western blotting with the indicated antibodies. Annexin A2 (ANXA2) was used as equal loading marker. Note the decrease of LC3 lipidation upon Vps34 or Beclin1 down-regulation in lipid micelle–treated cells. (B) Confocal analysis of Caco-2/TC7 enterocytes transfected with mock RNAi (siCTRL), RNAi for hVps34 (siVps34), or hBeclin1 (siBeclin1) as in A and treated with fluorescent fatty acid (FA^{568})–containing lipid micelles for 10 min or 24 h before fixation and labeling with DAPI. (C) Bar diagrams showing the quantification of FA^{568} content in LDs (*nv*/1000 µm^2) in the indicated conditions in cells treated as in A and B. Values denote means ± SEM ($n = 3$ independent experiments; $p < 0.001$). (D) Total membranes and LD fractions were recovered after postnuclear supernatant ultracentrifugation (see *Materials and Methods*) from Caco-2/TC7 enterocytes transfected with hBeclin1 (siBeclin1) or control siRNA (siCTRL) and supplied or not with lipid micelles for 24 h (mic. 24 h). Equal volumes of the fractions were analyzed by Western blotting with anti-CLNX antibody as an ER marker and PLIN2/ADRP as a LD marker. (E) TG quantification from Caco-2/TC7 enterocytes transfected with control RNAi (siCTRL) or hBeclin1 siRNA (siBec) and supplied or not with lipid micelles for 24 h. TGs were quantified from the LD fraction collected upon flotation of the postnuclear supernatant as in D. TGs are expressed as nanomoles/milliliter, and values denote means ± SEM ($n = 3$ independent experiments; $p < 0.001$).

Inhibition of autophagy primary steps increases lipid droplet content and favors high-density lipoprotein secretion

To further document the implication of autophagy in the fate of newly formed LDs in enterocytes, we blocked autophagosome formation by knocking down beclin1 and Vps34, both key players in autophagy pathway initiation (Zeng *et al.*, 2006; Cao and Klionsky, 2007; Simonsen and Tooze, 2009). Lipid micelle–induced lipidation of LC3 was no longer detectable in Caco-2/TC7 cells transfected with small interfering RNA (siRNA) targeting beclin1 or Vps34 (Figure 8A), indicating that lipid micelle–associated autophagy was blocked. To assess the effect of the inhibition of autophagy on the LD formation and evolution, we supplied siVps34 or siBeclin Caco-2/TC7 cells with FA^{568}-micelles for a short 10-min period to promote LD biogenesis or a longer 24-h period to promote LD biogenesis and accumulation. We did not observe any difference in FA^{568}-LD content in siVps34- or siBeclin1-transfected cells as compared with control cells after 10 min of lipid micelle supply. However, the FA^{568}-LD content significantly increased in siVps34- and siBeclin1-treated cells after 24 h of lipid micelle treatment (Figure 8, B and C). Similar results were obtained in cells down-regulated for ATG5, which is essential to autophagosome maturation (Boya *et al.*, 2013) without being dependent on PI3P synthesis as are Beclin1 and Vps34 (Supplemental Figure S8A). These data argue for an accumulation of LDs as a consequence of a blockade of autophagy primary steps. Accordingly, PLIN2, one of the main coat proteins of LDs, was strongly increased in LD fractions isolated from siBeclin1-transfected cells as compared with control cells (Figure 8D). Finally, we biochemically showed accumulation of TGs in LD fractions from siBeclin1-treated compared with control cells (Figure 8E), notably after 24 h of lipid micelle supply, which correlated with PLIN2 increase in the same fraction (Figure 8D).

The TG pools that we measured directly (FA^{568}) and indirectly (BODIPY) by light microscopy or cellular fractionation (LD flotation) reflect solely the neutral lipids stored in the cytosol, whereas TGs are also distributed along the biosynthetic pathway, most probably associated with the ER, in the lumen (for future secretion via the biosynthetic pathway) and/or within the membrane(s) bilayer (Khandelia *et al.*, 2010; Sturley and Hussain, 2012). To get a more complete characterization of the effect of autophagy inhibition on the whole neutral lipids in enterocytes, we analyzed both the secreted and intracellular lipids (TG and phospholipids [PLs]) from control cells and cells knocked down for Beclin1. Surprisingly, we first noticed that total cellular TG content was not modified in siBeclin1 cells compared with

control cells, with or without lipid micelle treatment (Supplemental Figure S9A), whereas we did observed clear TG accumulation in isolated LD fractions of siBeclin1 cells compared with control cells (Figure 8E). Similarly, using [1-^{14}C]-labeled oleic acid (OA) as a radioactive tracer in lipid micelles to monitor newly synthesized lipids (including TG, cholesterol esters, and PLs), we did not observe any difference in labeled TG measured from cell lysates and basolateral medium of control and siBeclin1 cells (Supplemental Figure S9, B and E). Whereas no significant difference was observed for [1-^{14}C]-OA–labeled PLs in cell lysates, their secretion was significantly increased in siBeclin1 cells (Supplemental Figure S9C). This was accompanied by an increase of apolipoprotein A1 (ApoA1) secretion in the basolateral medium and in the purified high-density lipoprotein (HDL) fraction upon lipid micelle treatment in siBeclin1 cells (Supplemental Figure S9D). We also observed an increase of intracellular [1-^{14}C]-OA–labeled cholesterol esters in siBeclin1 cells (Supplemental Figure S9E, CE), which may result from an increased content of cholesterol that is therefore stored as cholesterol esters. Both results suggest that autophagy inhibition leads to increased secretion of HDL (Rader, 2006) in the medium. ApoA4, an apolipoprotein associated with ApoB-containing, TG-rich lipoproteins (Stan *et al.*, 2003), was not altered in cell lysates or cell media from siBeclin1 cells (Supplemental Figure S9D and unpublished data, respectively). In the absence of autophagy (siBec), cellular ApoB48 was up-regulated in control condition and down-regulated when lipid micelles were applied (Supplemental Figure S9D), arguing for a tight and complex relationship between ApoB turnover, LD homeostasis, and autophagy, as previously suggested (Fujimoto and Ohsaki, 2006; Ohsaki *et al.*, 2006, 2008). However and more important, secreted ApoB48 was strongly reduced in siBeclin1 cells (Supplemental Figure S9D). Given that in the intestine each TG-rich lipoprotein is structured by one molecule of ApoB48 (Hussain *et al.*, 2005), our data could reflect a default in TG-rich/ApoB-containing lipoprotein secretion in the absence of autophagy. Together these results indicate that autophagy inhibition leads to TG accumulation as intracellular LD and accumulation of cholesterol esters and may have a mild effect on secreted triglyceride-rich lipoproteins accompanied by increased production of HDL by enterocytes.

DISCUSSION

We report here for the first time that delivery of alimentary lipids to human enterocytes induces a specific autophagic response, with the targeting of cytosolic LDs to lysosomes as a consequence (see summary scheme, Supplemental Figure S10). Enterocyte LDs are heterogeneous in size and subcellular localization, and this "multiple-pool" situation is due to growing and trafficking events starting after LD biogenesis at the ER membrane and requiring fusion and microtubules to stock large amounts of neutral lipids as large basal LDs. In parallel to this cytosolic lipid stock formation, almost half the population of LDs is taken in charge by autophagy machinery, leading to TG targeting to lysosomes. One novel aspect of the present study is the description of an ER-membrane located process through which newly synthesized, still basically ER-associated LD are captured by nonmature autophagosomal structures positive for PI3P, which will grow up as mature autophagosomes. Thus the structures that we observed at equilibrium comprising neutral lipids and markers for autophagosomes and late endosomes/lysosomes do not result from fusion of mature LD and mature autophagosome but rather from a local meeting at ER membrane, where both LDs and autophagosomes originate. Of importance, persistence of these structures may reflect a permanent autophagic state due to constant lipid micelle delivery.

More than a decade of research on LDs has revealed their multiple roles in numerous physiological situations, in different cell types and organs, and even in different organisms, making them a bona fide intracellular dynamic organelle interacting with its environment rather than fat inert sacs, as they were described for years (Farese and Walther, 2009). An extensive literature is available on roles and characteristics of LDs in hepatocytes, adipocytes, and macrophages, but enterocyte LDs remained poorly studied despite their major contribution to the polarized transfer and metabolism of dietary lipids in intestinal epithelium (Demignot *et al.*, 2013). We described the study of enterocyte LDs via a proteomic approach, which revealed that, as suggested for adipocyte and hepatocyte LDs (Brasaemle *et al.*, 2004; Fujimoto *et al.*, 2004), enterocyte LDs are adapted to enterocyte functions, mainly lipid metabolism (Bouchoux *et al.*, 2011; Beilstein *et al.*, 2013). Here we describe the "early life" of LDs in enterocytes after alimentary lipid supply. Small LDs appear almost instantly at the ER surface and stay connected to the ER network while growing in size. Later, these perinuclear LDs will be transported to the basal pole of the cell via microtubules and fuel a stock of neutral lipids constituting basal LDs, presumably by fusion of dynamic perinuclear LDs.

Concomitant to the LD biogenesis, lipid micelle supply induces a prompt autophagic response as monitored by LC3 staining and LC3II biochemical analyses. This is accompanied by up-regulation of pivotal autophagy regulators and perturbation of the mTOR signaling that confirmed the specific autophagic process, as well as by an immediate enrichment in PI3P-positive structures, presumably autophagosomes, at the ER membrane surface and vicinity. How this specific autophagy induction is triggered by lipid micelles in enterocytes remains an open question.

We analyzed the effect of enforced autophagy on LD populations and behavior. We showed that starvation-induced autophagy decreases preexisting as well as newly synthesized LD contents after lipid micelle supply. Because autophagy's main function is to deliver cargo(es) to lysosome for degradation, we showed that the lysosomal acid lipase is required for the control of TG amount in our system. Pharmacological inhibition of this enzyme mimicked the abolition of lysosomal maturation obtained upon bafilomycin A1 treatment, considered as a late-autophagy inhibitor, and led to LD accumulation in the cytosol, suggesting that the fate of a subset of LDs is to be handled by lysosomes, as already suggested in other models (Christian *et al.*, 2013).

RNAi-mediated down-regulation of Vps34, Beclin1, or ATG5, three major actors in the primary steps of the autophagy cascade (Cao and Klionsky, 2007; Axe *et al.*, 2008), had robust consequences on neutral lipid distribution within the cell: the inhibition of autophagosome formation leads to massive accumulation of TGs as LDs. Results obtained from lipid and lipoprotein secretion analyses in cells with impaired autophagosomes indicate that ApoB48-containing lipoprotein secretion is diminished, although TG secretion is not modified and HDL production is increased. These results raise more general questions concerning the effect of long-term modulation of autophagy (beyond the scope of the primary steps of autophagy as explored in the present study) on intestinal lipoprotein assembly and secretion, which will be of interest in the future.

LDs have previously linked to autophagosomes and were shown to harbor LC3 (Shibata *et al.*, 2009) and associate with autophagosomes and autophagolysosome markers in hepatocytes (Singh *et al.*, 2009; Vescovo *et al.*, 2012); consistently, we observe clear and dynamic LD association with autophagy-related organelles in enterocytes. We show, moreover, that LD capture by autophagosomes, which formation is instantly activated by lipid micelles, is an early event occurring in ER domains positive for PI3P at LD birth sites. Of importance, our data suggest that the ER, which is a central trafficking, signaling, and membrane-remodeling station, not only has the

capability to initiate formation of LDs, presumably to avoid TG accumulation in the bilayer, but also allows autophagosome biogenesis in the same membrane area and in the same time frame.

The lipid-induced autophagy that we describe in enterocytes seems to be maintained with time, since we observed LD-autophagosome or LD-autophagolysosome structures long after lipid micelle supply, as well as sustained LC3 lipidation. This differs from starvation-induced autophagy, and deciphering whether this "permanent autophagy induction" could be directly linked to the presence of TG in the ER membrane will thus be of primary importance.

The delivery of lipid micelles to enterocytes is known to induce lipoprotein formation–related events (Morel *et al.*, 2004; Chateau *et al.*, 2005), and we previously identified the scavenger receptor SR-BI/CLA1, located at the enterocyte plasma membrane, as a pivotal signaling relay for some of these ER-associated processes, together with ERK and p38/MAPK (Beaslas *et al.*, 2009). Thus the study of potential interconnection(s) of SR-BI and autophagy signaling pathways is an attractive direction of future study.

One may hypothesize that despite their primary lysosomal-delivery function, autophagosomes could also be used as a "hiding" compartment in the cell, to avoid major TG accumulation in the biosynthetic pathway's membranes, a phenomenon favored by massive alimentary lipid uptake in enterocytes. Accordingly, autophagy has also been suggested to be connected to ER stress, potentially to protect cells (Fritz *et al.*, 2011; Benbrook and Long, 2012; Deegan *et al.*, 2013). Because the ER deals with acute and massive amounts of triglycerides in enterocytes and these lipid supplies may trigger ER stress (Chen *et al.*, 2011), it is tempting to hypothesize that enterocyte ER could initiate a multiple signaling and membrane-remodeling program, including and potentially linking LD biogenesis, autophagosome formation, and lipoprotein assembly. Such a local program could act as a global protection/adaptation response to the acute arrival of neutral lipids, a situation that enterocytes face during the postprandial phase. It can thus be linked directly with serum lipid levels and more globally with hypertriglyceridemia and subsequent risky cardiovascular situations (Miller *et al.*, 2011).

MATERIALS AND METHODS

Animals, treatments, and isolation of intestinal epithelial cells

Male C57BL/6 mice (6–8 wk) were purchased from Charles River (Chatillon-sur-Chalaronne, France). Mice were maintained in a 12-h light/12-h dark cycle and fed a chow diet (AO3, SAFE). All experimental procedures conformed to the guidelines for animal studies of the Animal Care and Use Committee (CREEA Ile de France No. 3, agreement p3-2008-30). Experiments were performed on fed animals with ad libitum access to water. Mice were force fed with 150 µl of water or olive oil, and intestinal epithelial cells were harvested 180 min after the lipid bolus. The jejunum (10 cm of intestine starting at 2 cm after the pylorus) were excised, and epithelial cells were isolated using cell recovery solution (BD Biosciences, Le Pont de Claix, France) as previously described (Frochot *et al.*, 2012). Intestinal epithelial cells were treated with lysis buffer containing 5% protease inhibitor cocktail (Sigma-Aldrich, Lyon, France), 20 mM Tris-HCl, pH 7.4, 1% Triton X-100, 5 mM EDTA, and 0.15 M NaCl and centrifuged (10 min, 13,000 rpm at 4°C) before Western blot analysis.

Cell culture, siRNA transfection, and lipid supply

Caco-2/TC7 enterocytes (Chantret *et al.*, 1994) were plated at a density of 0.25×10^6 cells/filter (23.1-mm diameter; Becton Dickinson) and grown as described (Morel *et al.*, 2004) for differentiation. When appropriate, Caco-2/TC7 cells were transfected in suspension with siRNAs for human Vps34 (SI00040950 and SI00040971; Qiagen, Courtaboeuf, France), human Beclin1 (S100055573 and S100055580; Qiagen), human ATG5 (S102633946 and S100069251; Qiagen), or human ATG14 (S104266878 and S100455574; Qiagen) using Lipofectamine 2000 (Invitrogen, Saint Aubin, France) and then plated at high density (3×10^6 cells/filter). Lipid micelles (2 mM sodium taurocholate, 0.6 mM oleic acid, 0.2 mM lysophosphatidylcholine, 0.05 mM cholesterol, and 0.2 mM 1-*O*-octadecyl-rac-glycerol, a stable analogue of monoacylglycerol) were prepared in serum-free medium as previously described (Pauquai *et al.*, 2006) and added to the upper compartment of differentiated cells for indicated times after 18 and 6 d of culture for low- and high-density seeded cells, respectively. When appropriate, lipid micelles were supplemented with 1 µCi of [1-^{14}C]oleic acid/ml of final medium as described (Chateau *et al.*, 2005). Cytotoxicity was assessed by the determination of LDH release in cell culture media using Cytotoxicity Detection Kit^{PLUS} (Roche, Meylan, France) according to the manufacturer's instructions.

Antibodies and reagents

The following antibodies were used: sheep polyclonal antibody to PLIN2/ADRP (for Western blots) was generously provided by J. McLauchlan's laboratory (Glasgow Caledonian University, Glasgow, United Kingdom). Mouse monoclonal anti-PLIN2 (for immunofluorescence) and guinea pig anti-PLIN3/TIP47 antibodies were from Progen. Mouse monoclonal antibodies to CLNX, early endosome auto-antigen 1 (EEA1), annexin A2 (ANXA2), E-cadherin (E-CADH), and lysosomal-associated membrane protein 1 (LAMP1) were from BD Biosciences. Rabbit polyclonal antibody to human ApoA1 was from Calbiochem (Molsheim, France). Mouse monoclonal anti-ApoB antibody was obtained from the Heart Institute of the University of Ottawa (Ottawa, Canada). Rabbit anti–ApoA-IV antibody was generously provided by M. Zakin (Pasteur Institute, Paris, France). Rabbit polyclonal antibody to microtubule-associated 1 light chain 3 (LC3; for Western blots) was from MBL (Nanterre, France). Mouse monoclonal antibody to LC3 (for immunofluorescence) was from Novus Bio (Cambridge, UK). Mouse monoclonal antibody to actin was from Millipore (Molsheim, France). Rabbit polyclonal antibodies to beclin1, LAMP1, and ATG14 and FITC–anti-GST goat antibodies were from Abcam (Cambridge, UK). Rabbit polyclonal antibody to ULK1 was from Santa Cruz Biotechnology (Nanterre, France). Rabbit polyclonal antibodies to P70-S6kinase, phospho-P70-S6kinase (Thr-389), phospho-ULK1 (Ser-757), Vps34/PIK3CIII (PI3 kinase class III), and EGFR were from Cell Signaling. Rabbit polyclonal antibody to ATG5 was from Abgent (Paris, France).

The chemicals and drugs used were as follows: FYVE-FYVE^{GST} recombinant protein was a kind gift from H. Stenmark's laboratory (Olso University Hospital, Oslo, Norway). Lysosomal acidic lipase inhibitor compound 12 LAListat2 (referred to as LALi) was a kind gift from P. Helquist's laboratory (Notre Dame University, Notre Dame, South Bend, IN). Alexa–phalloidin and wortmannin (100 nM final) were from Invitrogen. BODIPY 493/503 and C_{12}-fatty acid 568 nm (6 µM final concentration in lipid micelles) were from Molecular Probes. Digitonin, nocodazole (33 nM final), and bafilomycin A1 (100 nM final) were from Sigma-Aldrich. HBSS (with Ca^{2+} and Mg^{2+}) and insulin-transferrin-selenium medium (1000 mg/l insulin, 550 mg/l transferrin, and 0.67 mg/l selenium) were from Life Technologies (Saint Aubin, France).

Confocal fluorescence microscopy and image analysis

Caco-2/TC7 cells were fixed with 4% paraformaldehyde (PFA), permeabilized by 0.05% saponin or 0.01% digitonin (for LC3 staining) in

phosphate-buffered saline (PBS)/10% serum, incubated with primary antibodies in the same buffer, and then rinsed in PBS and incubated with appropriate cyanin dyes or Alexa Fluor–conjugated fluorescent secondary antibodies (Invitrogen). When indicated, cells were stained for neutral lipids with BODIPY 493/503 (10 µg/ml). For the labeling of PI3P with FYVE-FYVE^{GST}, cells were fixed and incubated for 1 h with purified FYVE-FYVE^{GST} recombinant protein (20 µg/ml final concentration), washed with PBS, and labeled with a FITC-conjugated anti-GST antibody. After nuclear staining by DAPI and post-fixation with 4% PFA, samples were examined by laser scanning confocal microscopy (LSM 710 microscope; Carl Zeiss). All confocal acquisitions, at subapical, nuclear, or basal plans, were analyzed (lipid droplet diameter, 3D reconstructions, *XZ* projections, etc.) with ZEN software (Carl Zeiss). Lipid droplets and/or number of autophagosome/endosome structures were manually counted in confocal sections (1000 µm^2). The value of total lipid droplet content used throughout this article corresponds to *n* (number of lipid droplets/1000-µm^2 cell field) × *v* (mean volume, in µm^3, of lipid droplets in the same area) and is expressed as arbitrary units.

Electron microscopy

Cells were processed for electron microscopy and stained for lipids by the imidazole-buffered osmium tetroxide procedure (Angermuller and Fahimi, 1982). Briefly, Caco-2/TC7 cells were fixed for 60 min with 2.5% glutaraldehyde in 0.1 M cacodylate buffer (pH 7.4) and then incubated for 30 min in 0.2 M imidazole buffer (pH 7.4) to which 4% aqueous osmium tetroxide was added immediately before use. All material was dehydrated with ethanol and embedded in Epon 812. Ultrathin sections were counterstained with 3% lead citrate for 60 min and examined with a Jeol 100CX-II electron microscope.

Protein and lipid biochemistry, fractionation, and immunoblotting

For Western blots analysis, cells were lysed for 10 min at 4°C in TNE (20 mM Tris, 150 mM NaCl, 1 mM EDTA, pH 7.4)–1% NP40 lysis buffer with protease inhibitor cocktail. For lipid analysis, cells were lysed with Triton lysis buffer (1% Triton X-100, 5 mM EDTA in PBS) supplemented with 2% protease inhibitor cocktail and centrifuged for 15 min at 12,000 rpm. Proteins in the supernatant were separated by SDS–PAGE, followed by a transfer onto nitrocellulose membranes. Total membranes and LD fractions were respectively recovered from the top and pellet after centrifugation (70,000 rpm, 30 min, 15°C) of postnuclear supernatant prepared with 3 mM imidazole and 8% sucrose. Protein concentration was determined by the Bio-Rad DC protein assay with bovine serum albumin as standard. Quantification of triglyceride content was performed using the PAP150TG kit (Biomerieux, Craponne, France) according to the manufacturer's instructions, with slight modifications. Briefly, after solvent evaporation, dried lipids were sonicated in 0.5 ml of the buffer provided before the addition of 0.5 ml of the twofold-concentrated kit reagent. Absorbance was measured after 1 h of incubation at 37°C. For analysis of lipid classes present in homogenates, supernatants, and fractions, lipids were extracted with chloroform/methanol (2:1 [vol/vol]) and separated by TLC as previously described (Chateau *et al.*, 2005). Radioactive bands were excised, and radioactivity was quantified by scintillation counting to evaluate the incorporation of [1-^{14}C]oleic acid into lipids.

HDL preparation

The collected basolateral media were immediately adjusted to 0.005% gentamicin, 1 mM EDTA, 0.04% sodium azide, and 0.02% sodium (ethylmercurithio)-2 benzoate. HDL isolation from other lipoproteins was performed by sequential ultracentrifugation according to their density (Havel *et al.*, 1955; Chateau *et al.*, 2005). Briefly, media were adjusted to a density of 1.063 and centrifuged at 100,000 × *g* at 10°C for 20 h. The upper fraction of the tubes, containing chylomicrons, very low density lipoprotein, and low-density lipoprotein, was discarded, and then the content was adjusted to a density of 1.21 and centrifuged at 100,000 × *g* and 10°C for 40 h. The top fraction, containing high-density lipoprotein, was collected, dialyzed against PBS, and analyzed for ApoA1 presence by Western blot.

Statistics

Data are presented as means ± SD or SEM. Statistical analyses were performed using Student's *t* test (*$p < 0.005$, **$p < 0.001$, and ***$p < 0.0001$).

ACKNOWLEDGMENTS

We thank P. Helquist, J. Gruenberg, H. Stenmark, M. Zakin, and J. McLauchlan for kindly sharing reagents with us. We thank C. Dall'Armi and G. Di Paolo for helpful advice and constant support. We warmly thank Z. Chamoun for critical reading of the manuscript and help with statistical analyses and our team colleagues for stimulating and fruitful discussions.

REFERENCES

Angermuller S, Fahimi HD (1982). Imidazole-buffered osmium tetroxide: an excellent stain for visualization of lipids in transmission electron microscopy. Histochem J 14, 823–835.

Axe EL, Walker SA, Manifava M, Chandra P, Roderick HL, Habermann A, Griffiths G, Ktistakis NT (2008). Autophagosome formation from membrane compartments enriched in phosphatidylinositol 3-phosphate and dynamically connected to the endoplasmic reticulum. J Cell Biol 182, 685–701.

Beaslas O, Cueille C, Delers F, Chateau D, Chambaz J, Rousset M, Carriere V (2009). Sensing of dietary lipids by enterocytes: a new role for SR-BI/CLA-1. PLoS One 4, e4278.

Beilstein F, Bouchoux J, Rousset M, Demignot S (2013). Proteomic analysis of lipid droplets from Caco-2/TC7 enterocytes identifies novel modulators of lipid secretion. PLoS One 8, e53017.

Benbrook DM, Long A (2012). Integration of autophagy, proteasomal degradation, unfolded protein response and apoptosis. Exp Oncol 34, 286–297.

Bouchoux J *et al.* (2011). The proteome of cytosolic lipid droplets isolated from differentiated Caco-2/TC7 enterocytes reveals cell-specific characteristics. Biol Cell 103, 499–517.

Boya P, Reggiori F, Codogno P (2013). Emerging regulation and functions of autophagy. Nat Cell Biol 15, 713–720.

Brasaemle DL, Dolios G, Shapiro L, Wang R (2004). Proteomic analysis of proteins associated with lipid droplets of basal and lipolytically stimulated 3T3-L1 adipocytes. J Biol Chem 279, 46835–46842.

Cao Y, Klionsky DJ (2007). Physiological functions of Atg6/Beclin 1: a unique autophagy-related protein. Cell Res 17, 839–849.

Chantret I, Rodolosse A, Barbat A, Dussaulx E, Brot-Laroche E, Zweibaum A, Rousset M (1994). Differential expression of sucrase-isomaltase in clones isolated from early and late passages of the cell line Caco-2: evidence for glucose-dependent negative regulation. J Cell Sci 107, 213–225.

Chateau D, Pauquai T, Delers F, Rousset M, Chambaz J, Demignot S (2005). Lipid micelles stimulate the secretion of triglyceride-enriched apolipoprotein B48-containing lipoproteins by Caco-2 cells. J Cell Physiol 202, 767–776.

Chen J, Li Q, Zhang Y, Yang P, Zong Y, Qu S, Liu Z (2011). Oleic acid decreases the expression of a cholesterol transport-related protein (NPC1L1) by the induction of endoplasmic reticulum stress in CaCo-2 cells. J Physiol Biochem 67, 153–163.

Christian P, Sacco J, Adeli K (2013). Autophagy: emerging roles in lipid homeostasis and metabolic control. Biochim Biophys Acta 183, 819–824.

Codogno P, Mehrpour M, Proikas-Cezanne T (2011). Canonical and non-canonical autophagy: variations on a common theme of self-eating? Nat Rev Mol Cell Biol 13, 7–12.

Deegan S, Saveljeva S, Gorman AM, Samali A (2013). Stress-induced self-cannibalism: on the regulation of autophagy by endoplasmic reticulum stress. Cell Mol Life Sci 70, 2425–2441.
Demignot S, Beilstein F, Morel E (2013). Triglyceride-rich lipoproteins and cytosolic lipid droplets in enterocytes: key players in intestinal physiology and metabolic disorders. Biochimie, S0300-9084(13)00231-9.
Ding WX, Li M, Chen X, Ni HM, Lin CW, Gao W, Lu B, Stolz DB, Clemens DL, Yin XM (2010). Autophagy reduces acute ethanol-induced hepatotoxicity and steatosis in mice. Gastroenterology 139, 1740–1752.
Di Paolo G, De Camilli P (2006). Phosphoinositides in cell regulation and membrane dynamics. Nature 443, 651–657.
Farese RV Jr, Walther TC (2009). Lipid droplets finally get a little R-E-S-P-E-C-T. Cell 139, 855–860.
Fritz T, Niederreiter L, Adolph T, Blumberg RS, Kaser A (2011). Crohn's disease: NOD2, autophagy and ER stress converge. Gut 60, 1580–1588.
Frochot V *et al.* (2012). The transcription factor HNF-4alpha: a key factor of the intestinal uptake of fatty acids in mouse. Am J Physiol Gastrointest Liver Physiol 302, G1253–G1263.
Fujimoto Y, Itabe H, Sakai J, Makita M, Noda J, Mori M, Higashi Y, Kojima S, Takano T (2004). Identification of major proteins in the lipid droplet-enriched fraction isolated from the human hepatocyte cell line HuH7. Biochim Biophys Acta 1644, 47–59.
Fujimoto T, Ohsaki Y (2006). Proteasomal and autophagic pathways converge on lipid droplets. Autophagy 2, 299–301.
Fujimoto T, Ohsaki Y, Cheng J, Suzuki M, Shinohara Y (2008). Lipid droplets: a classic organelle with new outfits. Histochem Cell Biol 130, 263–279.
Gillooly DJ, Morrow IC, Lindsay M, Gould R, Bryant NJ, Gaullier JM, Parton RG, Stenmark H (2000). Localization of phosphatidylinositol 3-phosphate in yeast and mammalian cells. EMBO J 19, 4577–4588.
Gruenberg J, Stenmark H (2004). The biogenesis of multivesicular endosomes. Nat Rev Mol Cell Biol 5, 317–323.
Havel RJ, Eder HA, Bragdon JH (1955). The distribution and chemical composition of ultracentrifugally separated lipoproteins in human serum. J Clin Invest 34, 1345–1353.
Hayashi-Nishino M, Fujita N, Noda T, Yamaguchi A, Yoshimori T, Yamamoto A (2009). A subdomain of the endoplasmic reticulum forms a cradle for autophagosome formation. Nat Cell Biol 11, 1433–1437.
Heaton NS, Randall G (2010). Dengue virus-induced autophagy regulates lipid metabolism. Cell Host Microbe 8, 422–432.
Hoekstra D, Tyteca D, van IJzendoorn SC (2004). The subapical compartment: a traffic center in membrane polarity development. J Cell Sci 117, 2183–2192.
Hussain MM, Fatma S, Pan X, Iqbal J (2005). Intestinal lipoprotein assembly. Curr Opin Lipidol 16, 281–285.
Kabeya Y, Mizushima N, Ueno T, Yamamoto A, Kirisako T, Noda T, Kominami E, Ohsumi Y, Yoshimori T (2000). LC3, a mammalian homologue of yeast Apg8p, is localized in autophagosome membranes after processing. EMBO J 19, 5720–5728.
Khandelia H, Duelund L, Pakkanen KI, Ipsen JH (2010). Triglyceride blisters in lipid bilayers: implications for lipid droplet biogenesis and the mobile lipid signal in cancer cell membranes. PLoS One 5, e12811.
Klionsky DJ (2007). Autophagy: from phenomenology to molecular understanding in less than a decade. Nat Rev Mol Cell Biol 8, 931–937.
Lindmo K, Stenmark H (2006). Regulation of membrane traffic by phosphoinositide 3-kinases. J Cell Sci 119, 605–614.
Mansbach CM, Siddiqi SA (2010). The biogenesis of chylomicrons. Annu Rev Physiol 72, 315–333.
Martin S, Parton RG (2006). Lipid droplets: a unified view of a dynamic organelle. Nat Rev Mol Cell Biol 7, 373–378.
Matsunaga K, Morita E, Saitoh T, Akira S, Ktistakis NT, Izumi T, Noda T, Yoshimori T (2010). Autophagy requires endoplasmic reticulum targeting of the PI3-kinase complex via Atg14L. J Cell Biol 190, 511–521.
Matsuo H *et al.* (2004). Role of LBPA and Alix in multivesicular liposome formation and endosome organization. Science 303, 531–534.
Miller M *et al.* (2011). Triglycerides and cardiovascular disease: a scientific statement from the American Heart Association. Circulation 123, 2292–2333.
Mizushima N, Levine B, Cuervo AM, Klionsky DJ (2008). Autophagy fights disease through cellular self-digestion. Nature 451, 1069–1075.
Mizushima N, Yoshimori T, Levine B (2010). Methods in mammalian autophagy research. Cell 140, 313–326.
Morel E, Demignot S, Chateau D, Chambaz J, Rousset M, Delers F (2004). Lipid-dependent bidirectional traffic of apolipoprotein B in polarized enterocytes. Mol Biol Cell 15, 132–141.
Nakatogawa H, Suzuki K, Kamada Y, Ohsumi Y (2009). Dynamics and diversity in autophagy mechanisms: lessons from yeast. Nat Rev Mol Cell Biol 10, 458–467.
Noda T, Matsunaga K, Taguchi-Atarashi N, Yoshimori T (2010). Regulation of membrane biogenesis in autophagy via PI3P dynamics. Semin Cell Dev Biol 21, 671–676.
Ohsaki Y, Cheng J, Fujita A, Tokumoto T, Fujimoto T (2006). Cytoplasmic lipid droplets are sites of convergence of proteasomal and autophagic degradation of apolipoprotein B. Mol Biol Cell 17, 2674–2683.
Ohsaki Y, Cheng J, Suzuki M, Fujita A, Fujimoto T (2008). Lipid droplets are arrested in the ER membrane by tight binding of lipidated apolipoprotein B-100. J Cell Sci 121, 2415–2422.
Ouimet M, Franklin V, Mak E, Liao X, Tabas I, Marcel YL (2011). Autophagy regulates cholesterol efflux from macrophage foam cells via lysosomal acid lipase. Cell Metab 13, 655–667.
Pan X, Hussain MM (2012). Gut triglyceride production. Biochim Biophys Acta 1821, 727–735.
Pauquai T, Bouchoux J, Chateau D, Vidal R, Rousset M, Chambaz J, Demignot S (2006). Adaptation of enterocytic Caco-2 cells to glucose modulates triacylglycerol-rich lipoprotein secretion through triacylglycerol targeting into the endoplasmic reticulum lumen. Biochem J 395, 393–403.
Rader DJ (2006). Molecular regulation of HDL metabolism and function: implications for novel therapies. J Clin Invest 116, 3090–3100.
Robenek H, Hofnagel O, Buers I, Robenek MJ, Troyer D, Severs NJ (2006). Adipophilin-enriched domains in the ER membrane are sites of lipid droplet biogenesis. J Cell Sci 119, 4215–4224.
Robertson MD, Parkes M, Warren BF, Ferguson DJ, Jackson KG, Jewell DP, Frayn KN (2003). Mobilisation of enterocyte fat stores by oral glucose in humans. Gut 52, 834–839.
Rosenbaum AI, Cosner CC, Mariani CJ, Maxfield FR, Wiest O, Helquist P (2010). Thiadiazole carbamates: potent inhibitors of lysosomal acid lipase and potential Niemann-Pick type C disease therapeutics. J Med Chem 53, 5281–5289.
Shibata M, Yoshimura K, Furuya N, Koike M, Ueno T, Komatsu M, Arai H, Tanaka K, Kominami E, Uchiyama Y (2009). The MAP1-LC3 conjugation system is involved in lipid droplet formation. Biochem Biophys Res Commun 382, 419–423.
Simonsen A, Tooze SA (2009). Coordination of membrane events during autophagy by multiple class III PI3-kinase complexes. J Cell Biol 186, 773–782.
Singh R, Cuervo AM (2012). Lipophagy: connecting autophagy and lipid metabolism. Int J Cell Biol 2012, 282041.
Singh R, Kaushik S, Wang Y, Xiang Y, Novak I, Komatsu M, Tanaka K, Cuervo AM, Czaja MJ (2009). Autophagy regulates lipid metabolism. Nature 458, 1131–1135.
Skop V, Cahova M, Papackova Z, Palenickova E, Dankova H, Baranowski M, Zabielski P, Zdychova J, Zidkova J, Kazdova L (2012). Autophagy-lysosomal pathway is involved in lipid degradation in rat liver. Physiol Res 61, 287–297.
Stan S, Delvin E, Lambert M, Seidman E, Levy E (2003). Apo A-IV: an update on regulation and physiologic functions. Biochim Biophys Acta 1631, 177–187.
Stenmark H, Aasland R, Driscoll PC (2002). The phosphatidylinositol 3-phosphate-binding FYVE finger. FEBS Lett 513, 77–84.
Sturley SL, Hussain MM (2012). Lipid droplet formation on opposing sides of the endoplasmic reticulum. J Lipid Res 53, 1800–1810.
Thiele C, Spandl J (2008). Cell biology of lipid droplets. Curr Opin Cell Biol 20, 378–385.
Velikkakath AK, Nishimura T, Oita E, Ishihara N, Mizushima N (2012). Mammalian Atg2 proteins are essential for autophagosome formation and important for regulation of size and distribution of lipid droplets. Mol Biol Cell 23, 896–909.
Vescovo T *et al.* (2012). Autophagy protects cells from HCV-induced defects in lipid metabolism. Gastroenterology 142, 644–653 e643.
Walker S, Chandra P, Manifava M, Axe E, Ktistakis NT (2008). Making autophagosomes: localized synthesis of phosphatidylinositol 3-phosphate holds the clue. Autophagy 4, 1093–1096.
Weidberg H, Shvets E, Elazar Z (2009). Lipophagy: selective catabolism designed for lipids. Dev Cell 16, 628–630.
Xie Z, Klionsky DJ (2007). Autophagosome formation: core machinery and adaptations. Nat Cell Biol 9, 1102–1109.
Yamamoto A, Tagawa Y, Yoshimori T, Moriyama Y, Masaki R, Tashiro Y (1998). Bafilomycin A1 prevents maturation of autophagic vacuoles by inhibiting fusion between autophagosomes and lysosomes in rat hepatoma cell line, H-4-II-E cells. Cell Struct Funct 23, 33–42.
Yla-Anttila P, Vihinen H, Jokitalo E, Eskelinen EL (2009). 3D tomography reveals connections between the phagophore and endoplasmic reticulum. Autophagy 5, 1180–1185.
Zeng X, Overmeyer JH, Maltese WA (2006). Functional specificity of the mammalian Beclin-Vps34 PI 3-kinase complex in macroautophagy versus endocytosis and lysosomal enzyme trafficking. J Cell Sci 119, 259–270.